ENERGY EFFICIENT MODEL PREDICTIVE BUILDING TEMPERATURE CONTROL

ENERGY EFFICIENT
MODEL PREDICTIVE BUILDING TEMPERATURE CONTROL

by

Matt Wallace, B.Eng

A Thesis
Submitted to the School of Graduate Studies
in Partial Fulfillment of the Requirements
for the Degree
Master of Applied Science

McMaster University

MASTER OF APPLIED SCIENCE (2011) McMaster University

(Chemical Engineering) Hamilton, Ontario, Canada

TITLE:	Energy Efficient Model Predictive Building Temperature Control
AUTHOR:	Matt Wallace, B.Eng
	(McMaster University, Canada)
SUPERVISOR:	Dr. Prashant Mhaskar
NUMBER OF PAGES:	1, 75

ABSTRACT

Sustainability considerations have placed increasing emphasis on the energy efficient operation and control of temperature control systems. It is estimated that the use of advanced control structures could lead to valuable savings in energy expenditure (up to 15-20 %). This work considers the problem of developing a model predictive control (MPC) algorithm for temperature control in buildings. To this end, a cascade control structure was designed to regulate the room temperature subject to heat load disturbances, such as outdoor conditions or changes in the internal gains (i.e., number of people in a room). The inner loop of the cascade control structure involved controlling key variables of a vapor compression cycle (VCC), namely the superheat and supply air temperature (from the evaporator), by manipulating the compressor speed and valve opening (components in the VCC). Linear input-output models were appropriately identified for the VCC using a detailed first-principles model (adapted from Thermosys) for eventual utilization in a predictive control design. Then, closed loop simulations were performed by interfacing the VCC model with EnergyPlus (developed by the U.S. Department of Energy), which was used to model realistic room temperature behavior. The control performance using a predictive controller (in the inner loop) was then evaluated against PI control.

ACKNOWLEDGEMENTS

I wish to express my gratitude, first and foremost, to my supervisor Dr. Mhaskar, who has made my experience as a graduate student a positive one. His suggestions and aid in overcoming various challenges along the way to completing this research were greatfully appreciated and the quality and depth of this work was greatly aided by his input. His calm demeanour and thoughtfulness over the period of my research, aided greatly in being able to perform at a high level throughout various deadlines and stressful times.

The unwavering support of Siam, through his answers to my numerous questions, his feedback to my various suggestions and his direct assistance was greatly appreciated. His bluntness with respect to improving my research, design and communication abilities was imperative to my abilities improving over the period of my research.

The feedback and suggestions I received from Maaz, aided in the advancement of this research as well as it improved my understanding of control which I appreciate. Collaborating with Rahul, also was of great importance to the advancement of this research and my control knowledge. I greatly appreciated his feedback and research input for various questions and tasks associated with this work. Collaborating on the last stages of this work with Ryan, improved the quality and relevance of the results presented in this work and would not have been attainable without his dedication and work. I've learned much from his research and insight into this project which I greatly appreciate.

The frequent feedback and assistance received from Tim Salsbury and John House was essential in building my knowledge of refrigeration processes and their respective control. Also, obtaining industrial and energy relevant results would have been difficult without their input into this research.

Table of Contents

List of Figures

List of Tables

List of Symbols

Variable	Description
A	Area
α	Heat Transfer Coefficient
$\bar{\gamma}$	Mean Void Fraction
C_p	Specific Heat Capacity
D	Diameter
h	Specific Enthalpy
$\dot{m}$	Mass Flow Rate
m	mass
P	Pressure
ΔP	Pressure Drop
p	Perimeter
ρ	Density
T	Temperature
t	time
τ	Time Constant
V	Volume
w	Absolute Humidity

Subscript	Description
a	Air
avg	Average
c	Condenser
cs	Cross-Sectional
e	Evaporator
i	Inner
k	Compressor
l	Saturated Liquid
o	Outer
r	Refrigerant
v	Saturated Vapor
w	Wall
c,1	Condenser Superheat Region
c,2	Condenser Two-phase Region
c,3	Condenser Subcool Region
e,1	Evaporator Two-phase Region
e,2	Evaporator Superheat Region

Chapter 1

Introduction

Government regulations and energy costs have placed a large emphasis on reducing the energy consumption and improving the energy efficiency of various processes throughout Canada. This includes heating and cooling applications for the automotive, industrial and commericial sectors in Canada. Energy used for heating and cooling is classified as secondary energy, and a large portion of Canada's secondary energy is used in commericial/residential structures (Figure 1.1). The energy used in operating heating, ventilation and air-conditioning (HVAC) systems account for between 40 - 50 % of the total energy consumption of a building. Between 15 - 20 % of the total energy consumption can be reduced through more efficient operation of buildings [Behidj *et al.* [2009]].

Improving the operating efficiency of a building can take place at various times over a building's lifespan. Improvement strategies can be implemented prior to construction as well as on pre-existing structures. Using design standards which incorporate energy and environmental concerns (LEED certification standards) ensure that future buildings will be energy conservative. Retrofitting the building equipment and material with more energy efficient technology (EnergyStar certified) and/or improving the scheduling and control of HVAC units in a building can improve the efficiency of a pre-existing building. This thesis focuses on the latter improvement strategy which can be classified into detailed sublevels, beginning with improving the control of the cooling side of a HVAC unit, which will henceforth be

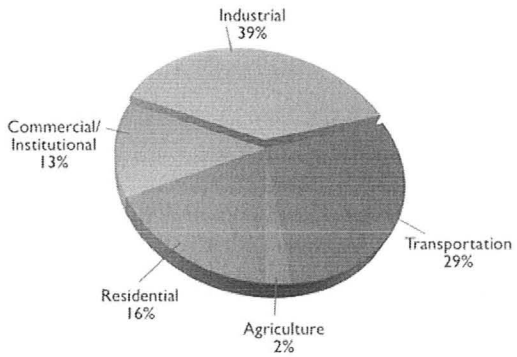

Figure 1.1: Distribution of Secondary Energy Usage in Canada [Behidj *et al.* [2009]]

referred to as a primary device, in the presence of common load variations. An intermediate sublevel includes improving the control of multiple primary devices accounting for building zone interactions. The final sublevel focuses on making the primary device startup/ shut down procedures more cost effective and less energy intensive. Future research will account for the intermediate and final sublevels of this improvement strategy.

A common primary device is a Vapor Compression Cycle (VCC), which is used to cool either an air or water medium. Traditional VCC control strategies have included PID/PI decentralized control and simple on/off control (both single-input-single-output (SISO) control structures) [Keir and Alleyne [2007]; Alleyne *et al.* [2009]]. Common input/output variables used in the SISO control structures have included using the compressor RPM, expansion valve opening and/or air fan speeds to regulate output variables such as evaporator superheat temperature, condenser pressure, evaporator pressure and/or evaporator supply air temperature. Using multiple SISO controllers to regulate multiple outputs has limited effectiveness due to the extensive interaction/cross-coupling of the nonlinear VCC dynamics. Centralized model predictive control (MPC) designs, on the other hand, offer improved control performance by accounting for these interactions (through a dynamic model of the process). Recent MPC formulations (e.g., see [Mhaskar [2006]; Mahmood and Mhaskar [2008]]) have addressed several fundamental feasibility and robustness issues, motivating the use of a predictive control design for HVAC units.

Recently, a considerable amount of research has been completed in the field of HVAC control, specifically in the area of MPC. A detailed literature review is completed in a subsequent section of this thesis. While previous work has shown improved energy efficiency and/or operating cost for specific HVAC units compared to traditional control strategies, the VCC model utilized in the system identification and/or control design has been over a limited range of operating conditions ([Sandipan *et al.* [2010]]) or consisted of a high number of nonlinear equations, making the resulting control formulation impractical for real-time implementation. Moreover, using a purely deterministic model in a MPC formulation makes the performance subject to several model parameters, many of which may be not be known accurately. Generally, when determining an appropriate predictive model for use in a MPC structure, a trade-off exists between the complexity and practical usefulness of the model. In this work, we opted for practical implementability and used an empirically identified autoregressive exogenous (ARX) model in the control design. The ARX model used in the control design can be readily built using commonly measured variables, allowing the implementation of the resulting MPC design on new/different cooling installations.

One issue that has received limited research attention in the control of VCC systems is evaluating the interaction between the performance of the cooling unit with time-weather-dependent heat loads associated with a common building (e.g., see [Ma *et al.* [2010a]], [May-Ostendorp *et al.* [2010]]). In this work, we address this issue by integrating the closed-loop VCC simulations with EnergyPlus, a popular simulation program used for investigating building energy efficiency. Although initially designed as a stand-alone program, recent advances have allowed EnergyPlus to be run in conjunction with other commercial simulation platforms [Crawley *et al.* [2001]; Wetter, M. and Haves, P. [2008]]. An original contribution of this work includes the evaluation of a predictive control design in regulating a VCC model when used in conjunction with a realistic building simulation provided by EnergyPlus which accounted for realistic weather considerations such as humidity. The specific contributions of the thesis are listed below.

Contributions

- Model selection for primary unit and building - selecting models that capture the dynamics of an actual primary unit and capture common variations associated with the air exposed to the different components in the primary unit.

- Improvements to the models

  Corrections - eliminating error in the calculation method used for the refrigerant mass flow rate at various locations in the primary unit and eliminating any discontinuity in flow parameters experienced if the primary unit model is operated outside the experimentally validate operating range.

  Enhancements - increasing the cooling capacity of the primary unit and implementing an evaporator model which incorporates the possibility of condensation occurring in the ambient air.

  Computation speed - converting the original primary unit model from multiple simulink blocks to a condensed m-file, improving the speed of simulations and eliminating any potential simulink-based issues associated with adjusting the original primary unit model or implementing non-simulink control strategies.

- Benchmarking control strategy - using a classical control strategy, which is common to industry, as the benchmark for comparing the closed-loop performance of the predictive control strategy against

- Model Identification and offset-free MPC design - using a model identification procedure which can be applied to various primary units to obtain the output model used in the predictive controller. Using a MPC design which can acheive off-set free tracking in the presence of plant-model mismatch over a range of operating conditions.

The most important contribution of this thesis is to build towards a framework that allows for real-time implementation of these strategies.

Chapter Description

- Chapter 2: Reviews pertinent literature including model identifications schemes, MPC

strategies and the regulation of energy systems with a variety of control strategies including MPC designs.

- Chapter 3: Describes the VCC, building models and the interfacing of these models, in addition to providing a general description of model predictive control.
- Chapter 4: Describes the corrections made to the VCC model and gives a detailed explaination of the design and implementation of both the classical and predictive control strategies. This includes an in-depth look at the model identification procedure and optimization problem formulation in the predictive controller design.
- Chapter 5: Provides the closed-loop results of each control strategy in regulating the stand-alone VCC and regulating the interfaced VCC system.
- Chapter 6: Concludes with a summary of the design and results of the predictive controller and also provides possible directions for future work that could stem from the work presented in this thesis.

Chapter 2

Literature Review

In this chapter a review of the results on the key components of the work is presented: model identification and model predictive control, with specific focus on the control of secondary energy systems in general and an indepth look into MPC of energy systems.

2.1 Model Identification

In Rake [1980] a variety of time varying input signals used for model identification of dynamic processes were described. Monofrequency and multifrequency sinusoidal or binary sequences are used for identifying frequency response models or parametric models. If the actual process dynamics are linear, a single step test can adequately capture the process dynamics at a variety of operating conditions, however if the process is considerable nonlinear, using one of the former periodic input sequences is advantageous to identifying different local dynamics associated with various operating conditions.

Rivera *et al.* [2009] developed a multi-sine input signal design procedure used for model identification and subsequent controller design. The design procedure constrained the amplitude of the sine signals and because the power associated with each sine wave was designated using a power spectrum, each input sine wave was independent and uncorrelated with the

others. This design method also allowed for modifications to be made to the power spectrum by the user to incorporate *a priori* process knowledge (ie. specific time or freqency-domain constraints). This input signal procedure was implemented on a high-purity distillation column, which is a highly nonlinear multi-variable process, and it was verified that the autoregressive exogenous (ARX) models identified from the input-output responses of the multi-sine procedure adequately represented the actual process dynamics.

Yuan and L. [1985] studied the problem of optimal input design used for estimating transfer functions of linear systems. The optimal input signals were chosen based on minimizing the mean square error of a quadratic norm term, evaluated in the frequency-domain. The error was defined as the difference between the actual linear system output and the output from the estimated transfer function. The identification procedure used for obtaining the input signals did not require any *a priori* knowledge of the actual linear system, however it was required that the true noise spectrum was known. The unprejudiced input signals were more robust to system properties compared to standard prejudiced input signal design, which allowed for the system output dynamics to be captured more accurately in the estimated transfer function.

Li and Georgakis [2008] used an iterative model identification procedure which updated the input test signals based on *a priori* output dynamics. Uncorrelated Pseudo-Random-Binary-Sequences (PRBS) were designed for each process input such that output constraints were not violated based on the *a priori* dynamic process model. Each input PRBS consisted of an oscillating signal which shifted between two values at varying periods. Once a new process model was obtained from the previous PRBS input-output data, the subsequent PRBS could be redesigned based on the updated model. A final model was determined based on comparing the value of a normalized sum of squared error term, where the error was the difference between subsequent estimated models. This identification method was implemented and verified to identify adequate models for the Tennessee Eastman problem.

Lin and Yeh [2007] used a specific input sequence to identify a bond-graph model for a vapor compression cycle (VCC). A more detailed description of the bond-graph model is

presented in Lin and Yeh [2002]. The VCC model was identified from a split-type residential air-conditioner with R-22 refrigerant where a square wave sequence was applied to the compressor RPM and expansion valve opening of the residential system. Initially, the compressor RPM was varied while the expansion valve was maintained at a constant value, followed by variations in the valve opening with a constant RPM value. Different frequency variations were applied to both inputs during this wave sequence. Through varying each input seperately, the individual effect of each input on different VCC outputs were isolated, allowing for an openloop model to be identified which captured unbiased dynamics between each input and output.

Chen *et al.* [2007] used a genetic algorithm (GA) to identify the coefficients and the number of lags in auto-regressive exogenous (ARX) models for both linear and nonlinear dynamic systems. A root mean square of the prediction error for all data points used in the model formulation and the speed of convergence were used as measures to quanitfy the performance of the GA process in identifying an ARX model. An original contribution of this work was obtaining the values of the ARX coefficients and number of lags through minimizing a specific fitness function. By using this new fitness function, it allowed for a more accurate ARX model to be formulated in less time compared to the time required to obtain the ARX model parameters through the minimization of the sum of the prediction error.

2.2 Model Predictive Control (MPC)

Garcia *et al.* [1989] provides a review and detailed description of the implementation of various model predictive control (MPC) designs. MPC designs have been used to solve both unconstrained and constrained optimization problems using either linear or non-linear models to predict the evolution of the state/output variables of various processes while determining the control trajectory for a process in terms of optimizing a predefined measure. This predefined measure usually incorporates specific state/output variable tracking error in addition to ensuring the control action satisfies predefined state/output/input constraints related to the operation of the actual process. Specific model predictive control

schemes have been designed which are robust to plant-model mismatch potentially caused by modifications to the process or poor model identification techniques initially being used.

Various processes have been regulated using both linear and nonlinear MPC designs including the work of Harnischmacher and Marqardt [2007] which looked into the control of a simulation-based fluid catalytic cracking (FCC) unit using a nonlinear MPC design to regulate the cracking severity through adjusting the air flow rate and the catalyst recirculation rate. To regulate the cracking severity, the riser outlet temperature was regulated about a desired setting. The nonlinear model used for the output predictions was a discrete-time Hamerstein model which consisted of individual sensitivity equations which were used in the optimization problem to find the optimal input values instead of using a finite difference approximation for the output gradients. The objective function being minimized consisted of quadratic terms penalizing the deviation of the riser outlet temperature from a respective set-point, a term penalizing the rate of change of the inputs (reducing process variability) and a term which penalized the absolute value of the inputs where this final term acted as an economic factor, as high air flow and catalyst recirculation rates correlate to higher expenses.

Linear MPC designs have also been deemed as effective controllers. Zhu *et al.* [2001] used a linear MPC design to regulate a simulated large-scale gas pipeline network which was highly nonlinear. The linear MPC structure was used to regulate specific pipeline pressures by adjusting production pressure set points of the cryogenic air separation plants connected to the pipeline. The linear model used in the control design was obtained by linearizing a nonlinear first principle model of the piping network about the nominal operating point of the pipeline. The discrete state-space model incorporated both measured and unmeasured output disturbances into the prediction of the system states. The unmeasured disturbances were estimated using a deadbeat observer. Three outputs were required to be maintained at specific setpoints, while 14 different outputs were to be maintained within constraints. Constraints on the system inputs were used to ensure realistic operating values for the cryogenic air plants. This linear MPC design was able to reject disturbances associated with cryogenic plant shutdown procedures while ensuring the outputs were maintained at

their desired setpoint values or within their desired constraints.

Mayne *et al.* [2000] completed a literature review of model predictive control designs of constrained systems that are both linear and nonlinear. From their review, they were able to determine stability principles which they used to characterize most of the model predictive controllers that had been proposed in the literature at the time of their publication. They were able to determine that some finite horizon optimization problems solved on-line were equivalent to the same problem solved using an infinite horizon and in other MPC designs it was applicable to a modified infinite horizon problem.

Muske and Badgwell [2002] designed an MPC framework which incorporated disturbance modeling to provide offset-free tracking using a linear model. The model predictive controller was able to drive and maintain the actual process outputs to desired setpoints through modeling unmeasured disturbances in the input, state and/or outputs of the process as dynamic models. The disturbance and state variables were estimated using a Kalman filter and to ensure offset-free tracking the state and disturbance model must be detectable as well as the number of unmeasured disturbances must be less or equal to the number of measured outputs. Offset-free tracking was obtained through regulating a simulation based distillation column using the aforementoined MPC framework.

Mhaskar [2006] developed a robust model predictive controller which could stabilize a nonlinear system subject to constraints, uncertainty and faults in the control actuator. The predictive controller was designed starting from a set of initial conditions (I.C.) where the feasibility of the optimization problem and the closed-loop stability was guaranteed. Constraints in the predictive controller were formulated using Lyapunov-based techniques which explicitly accounted for uncertainty in the predictive control law and which allowed for the I.C. set to be explicitly characterized starting from where the constraints are guaranteed initially and successively feasible. Using these constraints, a fault-tolerant controller was designed which used the knowledge of the stability regions from the originally designed controller to ensure the state trajectory stayed within these stability regions in both fault and non-fault operation of the system. This robust predictive controller was able to maintain

the state trajectory in the stability region for a simulated chemical reactor in the presence and in the absence of a faulty actuator.

Mhaskar and Kennedy [2008] developed a robust predictive controller which could stabilize affine nonlinear process systems subject to rate of change constraints and magnitude constraints for the control inputs in the presence of system uncertainty. A new robust predictive controller formulation was used which guaranteed stabilization from an explicit I.C. set, while minimizing the rate of change constraint violation. Based on the I.C. set, conditions were derived that enforced the rate constraints as hard constraints and a predictive controller was designed which enforced the rate constraints being satisfied if possible and preserving stability otherwise. This predictive controller was able to enforce rate constraints on the inlet concentration and heat supply which were the inputs for a simulated chemical reactor.

Maeder *et al.* [2009] also looked into offset-free tracking of a constant reference value using a linear MPC framework. A disturbance model was added to the state-space model used in the MPC framework to capture the plant-model mismatch and the states and disturbances were estimated using an observer design based on Pannochia and Rawlings [2003]. An original contribution of this work is for the case when the number of measured outputs is greater than the number of disturbance variables, an algorithm for computing the observer gaisn was developed which ensured zero-offset in specific output variables. Using this algorithm allowed the linear MPC controller to have less parameters, resulting in a less complex linear MPC offset-free design being achieved.

2.3 Control of Secondary Energy Systems

In Keir and Alleyne [2007], the regulation of a vapor compression cycle (VCC) using Proportional-Integral (PI) controllers was examined. Through a relative gain array analysis, it was determined that the traditional input-output (I/O) pairings for the feedback controllers, pairing the compressor RPM with the evaporator pressure and the expansion

valve opening with the evaporator superheat temperature were less effective than an alternative pairing scheme. The alternative pairing scheme consisted of the same superheat pairing in addition to using the compressor RPM to regulate the difference between the condenser pressure and the evaporator pressure. Using the alternative pairing scheme in the PI controllers reduced the coupling between the outputs of each controller, improving the controllability of the VCC.

Jain *et al.* [2010] regulated an experimental VCC using multiple single-input-single-ouput (SISO) control loops using a new method for identifying the I/O pairings for each controller. The inputs investigated in this analysis included the compressor RPM, expansion valve opening and the evaporator mass flow rate. The outputs explored were either individual or combinations of VCC outputs, where the output combinations had consistent units to ensure physical significance (ie. no pressure-temperature combinations). The field of possible I/O pairings were reduced initially using a relative gain array (RGA) number as a decoupling measure, then using engineering intuition and the number of incidents a specific I/O pairing was present in the reduced set of I/O pairings, the final I/O pairings were decided upon. Two different sets of I/O pairings were suggested where each set corresponded to operating the VCC with either a high or low frequency range of inputs. It was determined that through regulating combinations of VCC outputs, the system dynamics were further decoupled which allowed for more efficient regulation of the evaporator superheat and the supply air temperature relative to traditional I/O pairings.

The model identified in Lin and Yeh [2007] was a state-space model formulated about a specific operating point, where the superheat temperature, evaporator two-phase region temperature and the indoor temperature were state variables and the compressor RPM and valve opening were the inputs. The model was used to tune individual PI controllers using a linear quadratic (LQR) approach. A cascade control structure regulated the indoor temperature, using an outer PI controller to regulate the indoor temperature through adjusting the set point value of an inner PI controller which regulated the evaporator two-phase region temperature using the compressor RPM. The inner control loop also consists of a PI controller regulating the superheat temperature using the expansion valve opening.

To reduce the coupling between the inner control loops, a first-order decoupler was used to decouple the effect of the input signals before they were implemented on the VCC.

A linear-quadratic-Gaussian (LQG) controller as described in Schurt *et al.* [2009] was used to regulate an experimental VCC. The LQG controller was used to prescribe valve opening and compressor RPM values to the VCC which ensured the evaporator superheat was maintained at a predefined value in addition to satisfying desired cooling demands. A linear state-space model was obtained through linearizing a dynamic VCC model and the matrices of the linear model were used in obtaining the control action values from the linear-quadratic-regulator (LQR). To account for unmeasurable state values, a Kalman filter type state observer was used. The LQG controller was able to provide acceptable cooling demand tracking and also was able to reject a range of thermal load disturbances.

Xu *et al.* [2006] used a generalized-predictive-control (GPC) PID controller to regulate a cooling coil used in HVAC systems. The coil is used to cool return air which is used a cooling/heating medium to regulate the temperature of a zone in a building. To account for one set of PID tuning parameters not being optimal for all operating conditions, the GPC-PID obtained a new control action every sample time by minimizing a cost function with the PID tuning parameters as decision variables. The cost function consisted of the difference between the predicted output values and a desired temperature set point, where the predicted supply air temperatures from the coil were modeled using two Diophantine equations. It was seen that the GPC-PID controller was able to adequately reject static and dynamic disturbances quickly at various operating conditions relative to a traditional PID controller.

2.4 MPC of Secondary Energy Systems

Recently, a considerable amount of research has been completed in the field of HVAC control, specifically in the area of MPC. In [Leducq *et al.* [2006]], a nonlinear MPC design was used to regulate the cooling capacity and maximize the coefficient of performance (COP)

for an experimental VCC pilot plant (with water as the cooling medium) by manipulating the compressor RPM and the refrigerant (water) mass flow rates. The nonlinear model derived in [Leducq *et al.* [2006]] consisted of seven ordinary differential equations (ODEs), representing the mass and energy balances in both VCC heat exchangers. Meanwhile, in [Sandipan *et al.* [2010]], an experimental chiller network, consisting of two chillers and multiple external heat exchangers, was controlled using a linear MPC design. This experimental system emulated the chilled water loops used in a two-story building consisting of three separate zones per story. A linear state space model was used to predict the evolution of the actual chiller network states in the MPC design. An 8 hour load demand for the building zones was used as a constraint in the MPC formulation. In [Ma *et al.* [2010b]], a chiller-cooling tower network was controlled using a nonlinear MPC scheme. The control objectives were to satisfy the cooling load for all days of operations in addition to minimizing the electricity cost for the chiller and cooling tower.

Sarabia *et al.* [2007] used a non-linear model predictive controller (NMPC) to regulate the refrigeration system in a supermarket. The refigeration system consisted of the same layout of components used in a VCC, however a main difference that existed was the use of multiple valves and evaporators to provide cooling to different environments (ie. display cases). Also of importance in the refrigeration system was the use of discrete input values, resulting in the compressor being operated either as on/off and the valves being operated as either open or close. A dynamic nonlinear model which was based on fundamental mass and energy balances on the individual evaporator units was used in the MPC design for predicting the evolution of the air temperature in each display case as well as the suction pressure (pressure between each evaporator and the compressor). To aviod a a mixed-integer nonlinear program (MINLP) optimization problem being solved at each sampling time, the discrete variables (RPM and valve) were transformed into continuous variables through using the times when each input was either on/off over the control horizon as the decision variables in the optimization problem. The objective function being penalized consisted of quadratic terms penalizing the deviation of the air temperature in each display case from a desired setting as well as a quadratic term penalizing the deviation of the suction pressure from a desired setting. Constraints on the suction pressure and individual display

case air temperatures were used in the optimization problem to correspond to realistic operating conditions of a supermarket refrigeration system. The NMPC design was able to adequately regulate the display air case temperatures and suction pressure at desired setting for a simulated supermarket refrigeration system.

Xi *et al.* [2007] regulated an experimental HVAC using a NMPC design. The HVAC system consisted of a chiller as the primary unit which cooled a water medium which was subsequently sent to an air handling unit (AHU) where the zone air would be blown over the water to enable cooling of the air. The nonlinear model was developed from a support vector regression (SVR) modelling method and was used to regulate both the zone air temperature and the zone relative humidity through adjusting the supply air fan speed and the chilled water valve opening. The objective function being minimized consisted of individual quadratic terms penalizing the deviation of both the zone air temperature and relative humidity from a predefined setting. Constraints were implemented on the deviated input values to limit the operating space for the controller. For specific set point combinations for the zone air temperature and relative humidity the NMPC design was able to provide more effective setpoint tracking (faster convergence) than regulating the same experimental HVAC system with a fuzzy neural network. The improved performance of the SVR MPC method corresponded to the SVR having considerably smaller steady-state error in the zone air outputs compared to the steady-state values predicted using a fuzzy neural network.

Huang *et al.* [2009] developed a robust MPC design used for improving the temperature regulation of an air-conditioning system. The closed-loop performance was evaluated on a simulated variable air volume (VAV) AHU. A first-order with time-delay (FOTD) model was used to model the dynamics between the supply air temperature and the chilled water valve opening. Due to the high nonlinearity of an actual VAV AHU, a single FOTD model does not accurately represent the dynamics of the VAV AHU for its entire operating range. This motivated the use of a FOTD model where the process gain, time delay and time constant had uncertainty incorporated into their value, where the uncertainty of each parameter was bounded. A discrete version of the FOTD transfer function was used in the MPC design where the coefficients of the discrete model were combinations of the FOTD parameters. To

ensure the correct FOTD model was used in the MPC calculation, a polytope was used to determine the active FOTD model based on the current operating conditions (ie. output, input values). The objective function being minimized consisted of quadratic penalties on the supply air temperature deviation from a desired setting in addition to the rate of change of the valve opening. The control trajectory computed in the MPC was constrained to satisfy the physical constraints of the valve (ie. between 0 and 100 % open). The robust linear MPC design was able to reject disturbances in the return air temperature better than a conventional PID controller. This was evident due to the reduction in the oscillation magnitudes of the supply air temperature during both winter and summer days which incorporated varying return air conditions over a 20 hour test period.

Morosan *et al.* [2010] used a distributed MPC design to regulate the temperature of multiple zones in a building. Linear state space models accounted for the evolution of the zone air temperatures and were utilized in the control design to minimize a cost function emphasizing zone air temperature set-point tracking and low power consumption. Individual model predictive controllers were used to regulate the individual zone temperatures by determining values for the decision variables, heating power of each HVAC unit of the building, which minimized the local objective functions. Ma *et al.* [2010a] used a MPC design to determine the optimal zone temperature set points and power consumption of the individual HVAC units associated with a realistic building model. The MPC design used a linear model to predict the future zone temperatures and a weather estimator was incorporated to determine the daily cooling peak-demand period. By incorporating an estimate of future weather data into the control calculation, pre-cooling during non-peak periods allowed for the power consumed by the HVAC units of the building to be reduced compared with traditional pre-programmed HVAC unit control strategies.

Chapter 3

Preliminaries

The intent of this chapter is to describe the existing primary unit model, building model and the interconnecting software used for interfacing the models as well as providing a general description of a model predictive control approach.

3.1 Vapor Compression Cycle (VCC) Process

An ideal VCC contains four processes: isentropic compression in a compressor, isobaric energy dissipation in a condenser, isenthalpic expansion in an expansion valve and isobaric energy absorption in an evaporator [Rasmussen [2005]]. An overlay of a VCC on it's corresponding P-V diagram is displayed in Figure 3.1.

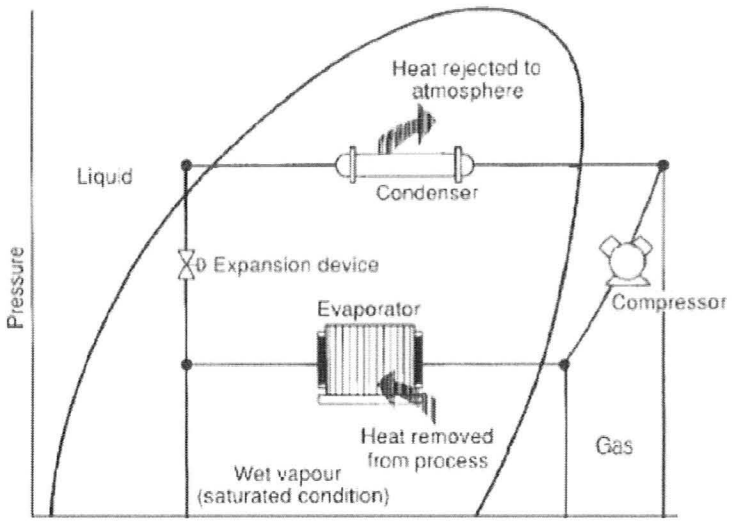

Figure 3.1: Pressure-Volume Diagram for VCC [India [2007]]

The refrigerant enters the compressor as superheated vapor and is compressed to a higher pressure resulting in the fluid having a higher temperature. The compression of the refrigerant ensures that the heat rejection side pressure is higher than the refrigerant pressure on the cooling side of the VCC, ensuring the refrigerant flows in the correct direction. From the compressor, the refrigerant enters an isobaric condenser with an ambient temperature below the temperature of the superheated refrigerant, resulting in the refrigerant condensing to a subcooled liquid at the condenser exit. The high pressure subcooled liquid then flows into an electronic expansion valve which decreases the pressure and temperature of the refrigerant causing a liquid-vapor mixture to form. Then, this two-phase refrigerant mixture enters an evaporator exposed to the medium being cooled. The environment temperature prior to cooling is above the temperature of the refrigerant causing the evaporation and subsequent heating of the refrigerant resulting in the formation of superheat at the evaporator exit. The air, in turn is cooled and available as primary air to be distributed for cooling. The superheated vapor from the evaporator exit then flows into the compressor, completing the cycle.

3.2 VCC Model

The VCC model was adapted from the Thermosys simulator developed at the Air Conditioning & Refrigeration Center (ACRC) at the University of Illinois at Urbana-Champaign. The expansion valve and piping were represented using static models and dynamic models were used for the condenser, evaporator and compressor.

3.2.1 Compressor

The VCC model used is based on the same processes as an ideal VCC except that the compression is not assumed to be a reversible, adiabatic process, instead it's defined using an isentropic efficiency [Rasmussen [2005]]. This is a valid assumption as the compression in an actual compressior is neither reversible or adiabatic due to non-zero values for the total work and total heat transfer caused by non-ideal mechanical factors such as friction and heat loss to the surroundings. The isentropic efficiency term, as defined in Equation 3.1, is the ratio of the work required for ideal adiabatic compression to the work required for actual compression.

$$\eta_k = \frac{h_{out,isentropic} - h_{in}}{h_{out} - h_{in}} \tag{3.1}$$

Another aspect which is not captured using the ideal VCC, is the volumetric limitations of the compressor, specifically that of a reciprocating compressor which is the compression unit modeled in the Thermosys-based VCC. A reciprocating compressor uses a cylinder-piston arrangement where a clearance volume exists between the piston and top of cylinder during compression. The purpose of the clearance volume is to eliminate contact between the piston and the cylinder. The difference between the clearance volume and the total cylinder volume, known as the swept volume, represents the actual region of compression (Figure 3.2).

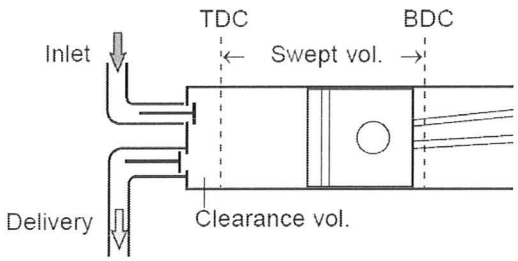

Figure 3.2: Reciprocating Compressor Cylinder Schematic [Grieve and Hughes [2010]]

After the compressed gas has been discharged, expansion occurs where the piston moves back to the bottom dead center position (BDC), increasing the region of compression and allowing for the induction of more gas. However, during this time the compressed gas in the clearance volume also expands, resulting in the induced gas volume being less than the swept volume, motivating the use of a volumetric efficiency term (η_{vol}) defined as the ratio of induced gas volume to the discharged gas volume (swept volume) [Grieve and Hughes [2010]].

The mass flow rate in the compressor is modeled using a static equation which is a function of η_{vol} (Equation 3.2). The $V_k \rho_k \eta_{vol}$ term represents the compressor capacity in terms of inlet refrigerant conditions and this quantity is multiplied by the compressor speed, ω_k, to provide a quantity defined as mass per unit time [Rasmussen [2005]].

$$\dot{m}_k = \omega_k V_k \rho_k \eta_{vol} \tag{3.2}$$

where V_k is the swept volume and ρ_k is the refrigerant density at the inlet.

In the VCC model, the η_{vol} and η_k values are obtained from lookup tables, populated based on efficiency term values obtained from an experimental VCC for various operating conditions. The experimental VCC used refrigerant r-134a to cool an air medium. The efficiency terms are dependent on the pressure ratio (P_{ratio}) of the outlet to inlet streams in the compressor and the compressor RPM (ω_k) (Equations 3.3- 3.4).

$$\eta_{vol} = f_1(P_{ratio}, \omega_k) \tag{3.3}$$

$$\eta_k = f_1(P_{ratio}, \omega_k) \tag{3.4}$$

With η_k values known, Equation 3.1 is rearranged to give an expression for an outlet refrigerant enthalpy (Equation 3.5).

$$h^*_{out} = \frac{1}{\eta_k}[h_{out,isentropic} + h_{in}(\eta_k - 1)] \tag{3.5}$$

This outlet refrigerant enthalpy is not the true value because the compressor consists of a shell containing the compression cylinder, resulting in Equation 3.5 not accurately representing $h_{k,out}$. After compression in the cylinder the refrigerant flows through the shell, prior to exiting the compressor, which consists of transport equipment/materials which were in contact with refrigerant at the previous compressed conditions. During the transport between discharging from the cylinder and exiting the shell the refrigerant enthalpy will vary due to heat tranfer between the refrigerant and the transport components. This motivated the use of a dynamic h_{out} model which accounts for this heat transfer in the transport section of the compressor (Equation 3.6).

$$\dot{h}_{out} = \frac{h^*_{out} - h_{out}}{\tau_{shell}} \tag{3.6}$$

h^*_{out} is obtained from Equation 3.5 and τ_{shell} is the compressor shell time constant.

3.2.2 Expansion Valve

The expansion valve is modeled as an isenthalpic process (Equation 3.8) with the mass flow rate a function of a discharge coeffcient (C_d) and pressure difference (ΔP = P_{in} - P_{out})

(Equation 3.7). C_d is determined using an experimental lookup table for the specific operating valve opening and ΔP (The density of the refrigerant (ρ) is defined as the maximum density of either the subcooled liquid density or the saturated liquid density at the inlet operating conditions). Both the subcooled and saturated liquid densities are obtained from lookup tables with reference values of inlet pressure and inlet enthalpy.

$$\dot{m}_v = C_d \sqrt{\rho \Delta P} \tag{3.7}$$

$$h_{v,in} = h_{v,out} \tag{3.8}$$

The VCC model is subcritical meaning that the pressure of the refrigerant leaving the compressor is below the critical point resulting in the refrigerant being incompressible (supercritical refrigerant is compressible) and forming an intermediate two-phase region in the condenser during the condensation of the refrigerant vapor [Rasmussen [2005]].

3.2.3 Heat Exchangers

The expansion valve and compressor dynamics are much faster than the heat exchanger dynamics, resulting in the VCC dynamics being dominated by the heat exchangers [Rasmussen [2005]]. The heat exchangers are modeled using a lumped parameter, moving boundary approach which accounts for the boundaries of the different fluid regions (superheated vapor, vapor-liquid, subcooled liquid) varying with time. Each fluid region is represented as a separate control volume with specific parameters (Figures 3.3 - 3.4).

Parameters from each fluid region are lumped together to form state variables (x). The lumping of parameters is accomplished by obtaining expressions for the refrigerant mass flow rate at the interface of adjacent regions in each heat exchanger and substituting these

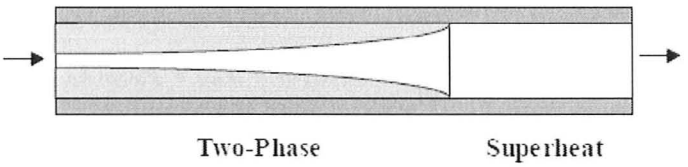

Figure 3.3: Evaporator with two fluid regions [Rasmussen [2005]]

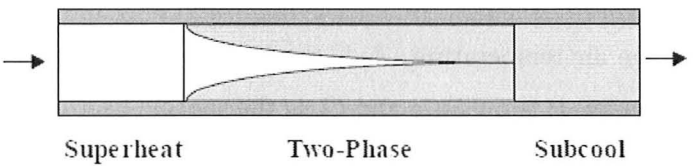

Figure 3.4: Condenser with three fluid regions [Rasmussen [2005]]

expressions into the ordinary differential equations (ODEs) that model the mass and energy balances of the heat exchanger. This reduces the number of ODEs and ensures no intermediate immeasurable variables are contained in the ODEs. The ODEs are formulated by integrating fundamental partial differential equations (PDEs), used for modeling fluid flow in a tube in each region of the heat exchangers. The heat exchanger is assumed to be a long horizontal tube and it is assumed that the pressure drop along the length of the heat exchanger is negligible, which makes the conservation of momentum PDE unnecessary. Equations 3.9 - 3.11 represent the refrigerant mass balance, energy balance and the wall energy balance of a specific fluid region.

$$\frac{\partial(\rho A_{cs})}{\partial t} + \frac{\partial \dot{m}}{\partial z} = 0 \tag{3.9}$$

$$\frac{\partial(\rho A_{cs} h - A_{cs} P)}{\partial t} + \frac{\partial(\dot{m} h)}{\partial z} = p_i \alpha_i (T_w - T_r) \tag{3.10}$$

$$(C_p \rho A)_w \frac{\partial T_w}{\partial t} = p_i \alpha_i (T_r - T_w) + p_o \alpha_o (T_a - T_w) \tag{3.11}$$

where p refers to the inner (i) and outer (o) perimeter of the single tube heat exchanger, α with subscript i (inner) and o (outer) are the heat transfer coefficients between the refrigerant and heat exchanger inner wall and between the heat exchanger outer wall and ambient air, respectively. T_w is the wall temperature, T_r is the refrigerant temperature and T_a is the average air temperature, A_c is the heat exchanger cross-sectional area , h is the refrigerant enthalpy, P is pressure and C_p is the specific heat capacity of the wall.

For the evaporator there are two fluid regions: a two-phase region followed by a superheat region, resulting in 5 PDEs. The condenser has three fluid regions: a vapor region followed by a two-phase and a subcooled region. This results in 7 PDEs being used to model the mass and energy balances of the condenser. In each two-phase region saturated liquid (f) and vapor (g) exist, causing the refrigerant fluid properties to be based on a weighted average of the saturated liquid and vapor properties. A mean void fraction ($\bar{\gamma}$) representing the fraction of total volume that is vapor, is used to determine the refrigerant fluid properties in the two-phase region (ie. $\rho = \rho_f$ (1-$\bar{\gamma}$) + $\rho_g \bar{\gamma}$, etc.). In the superheated and subcooled regions, the refrigerant enthalpy is an average property, assumed to be the average of the inlet and outlet enthalpies. This enthalpy is used with the refrigerant pressure to determine the density and temperature of the refrigerant in the region [Rasmussen [2005]]. The ODEs contain numerous partial derivative terms differentiated with respect to pressure as well as enthalpy because the fluid properties are a function of pressure and enthalpy and these parameters vary with time. The ODEs form a matrix structure in the form of Equation 3.12. This matrix structure is integrated at each time step, providing updated state variable values for both the evaporator and condenser.

$$Z(x,u) \cdot \dot{x} = f(x,u) \tag{3.12}$$

The state variables include: the length of the vapor ($L_{c,1}$) and two-phase ($L_{c,2}$) regions

in the condenser, the condenser wall temperatures in all three regions ($T_{c,w1}$, $T_{c,w2}$, $T_{c,w3}$) the condenser pressure (P_c), the condenser outlet refrigerant enthalpy ($h_{c,out}$), the length of the two-phase region in the evaporator ($L_{e,1}$), the evaporator wall temperatures for all regions ($T_{e,w1}$, $T_{e,w2}$), the evaporator pressure (P_e), the evaporator outlet refrigerant enthalpy ($h_{e,out}$) and the compressor outlet refrigerant enthalpy ($h_{k,out}$). The inputs are defined in terms of the compressor RPM, and valve opening (VO).

3.2.4 Evaporator

The original Thermosys Simulink VCC model accounts for the possibility of condensation occurring in the evaportor air as both temperature and humidity effects are incorporated in the evaporator model. There are two different methods used to calculate the outlet air temperature and humidity at the evaporator exit. The first method assumes that the water vapor in the air does not condense, resulting in only the temperature and not the absolute humidity, of the air changing. This change in air temperature is used in defining the sensible cooling load of the VCC.

The second method assumes a portion of the water content in the air condenses, resulting in the formation of a non-zero latent cooling load, in addition to a sensible cooling load.

Schematics for the condensing and non-condensing cooling cases are depicted in Figures 3.5 and 3.6, respectively.

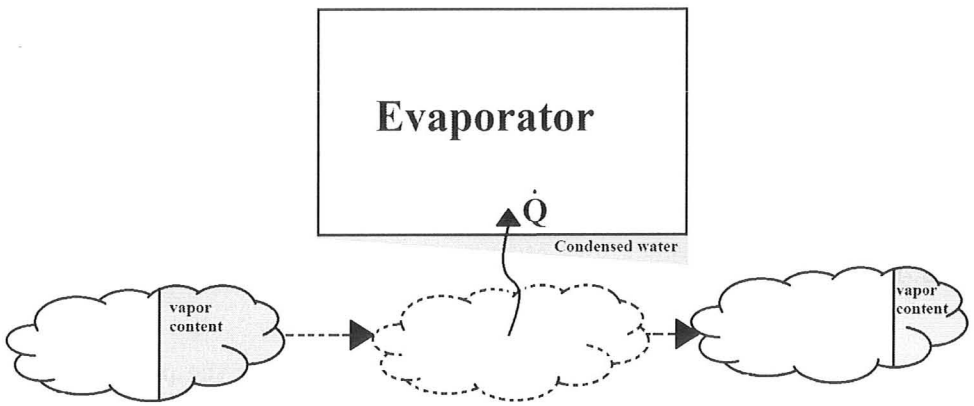

Figure 3.5: Evaporator Schematic with condensation

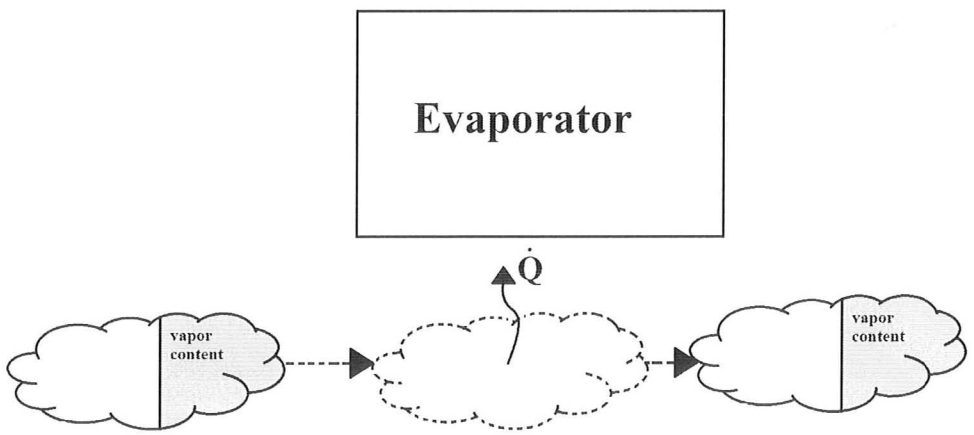

Figure 3.6: Evaporator Schematic without condensation

The equations used to obtain the outlet air temperature ($T_{air,out}$) are the wall side energy balance (Equation 3.13) which provides a value for the average air temperature, $T_{air,avg}$ and the $T_{air,avg}$ definition (Equation 3.14) which is rearranged to obtain a value for $T_{air,out}$.

$$\dot{m}_{dry\ air} C_{p,dry\ air}(T_{air,in} - T_{air,out}) + \dot{m}_{dry\ air}(w_{in} h_{in,water\ vap} - w_{out} h_{out,water\ vap}) = \alpha_{o,e} A_{o,e} \sum_{i=1}^{2} \frac{L_{e,i}}{L_{e,Total}} (T_{air,avg} - T_{e,wi}) \tag{3.13}$$

$$T_{air,avg} = \frac{1}{2}(T_{air,in} + T_{air,out}) \tag{3.14}$$

where w is the absolute humidity of the air at the inlet (in) and outlet (out).

3.3 Building Model

3.3.1 EnergyPlus Building Model

The MATLAB-based VCC model lacked realistic return and ambient air conditions, providing reason for interfacing the MATLAB VCC with additional software which would provide realistic air conditions. As previously mentioned, the EnergyPlus simulation package was used to provide return air conditions corresponding to an actual building and to provide ambient air conditions based on actual weather conditions for a specific American city.

For the EnergyPlus simulations used in this thesis, thermal simulations were carried out for a small (511 m^2), single story office building in Chicago, Illinois. The basic model, including building construction, surface geometries, and HVAC systems, were based on the U.S. Department of Energy (D.O.E) reference small office building model with minor adaptations to allow for proper interfacing with MATLAB [Deru *et al.* [2006]]. An isometric view of the office model is presented in Figure 3.7. The building is divided into five occupied

thermal zones, in which there is a conditioned floor area of 150 m^2 in the core zone, 113 m^2 in perimeter zones 1 and 3, and 67 m^2 in perimeter zones 2 and 4. The ground-to-ceiling height in all zones is 3 m. In total, the building houses 28 people at a standard occupant density of 5.38/100 m^2 per zone. The lighting and equipment internal gains for each zone were set to 10.76 W/m^2 and 8.07 W/m^2, respectively. During normal operation, the building is occupied between the hours of 6 : 00 and 20 : 00 with varying levels of occupancy.

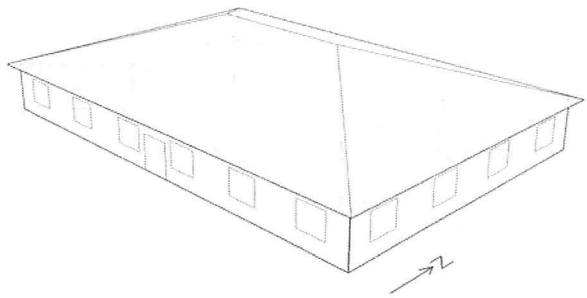

Figure 3.7: Schematic of EnergyPlus Small Office Building Model

In this work, the thermal environment of perimeter zone 2 was assumed to be regulated by the MATLAB VCC model with a 20 % fresh air intake. All remaining thermal zones were assumed to be controlled by separate air conditioning units modeled in EnergyPlus. To minimize the interaction between zones, the non-test zones were maintained at a constant set-point temperature of 24°C. The weather data used corresponded to the conditions of a common July day at Chicago O'Hare International Airport.

3.3.2 VCC-Building Model Interface

Data is exchanged between EnergyPlus and MATLAB over BSD sockets using the Building Controls Virtual Test Bed (BCVTB) middle-ware [Wetter, M. and Haves, P. [2008]]. The outdoor air temperature, zone air temperature, air pressure, and relative humidity are outputted to MATLAB for subsequent control calculations. MATLAB, in turn, provides a cooling output which is inputted into the EnergyPlus environment, as depicted in Figure

3.8.

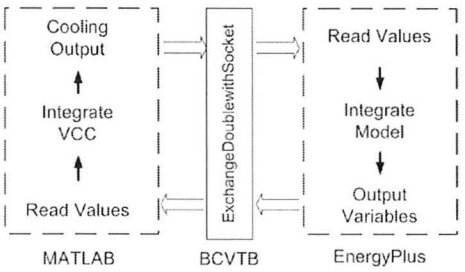

Figure 3.8: Schematic of EnergyPlus-MATLAB Interface

This data exchange between the two clients is accomplished using the exchangeDoublesWithSocket m-file provided in the BCVTB library. The exchangeDoublesWithSocket m-file reads a vector written to the BSD socket in BCVTB and overwrites a new vector onto the same socket. For this work, the exchangeDoubleswithSocket m-file reads a vector written to the socket from EnergyPlus and overwrites it with a cooling load vector generated in MATLAB. Following the exchange, the outputted MATLAB vector is passed through BCVTB and brought into EnergyPlus through an intrinsic external interface command. Over the course of a simulation, this data exchange occurs at the start of each time interval. To ensure that the simulation clients advance at the same rate, the overall time in the two models is not updated until both clients have completed the integration for the given time step. This progression occurs until the final time is reached in BCVTB, thereby triggering an end of simulation flag being sent to both clients to terminate the integration of both the VCC and the EnergyPlus model.

EnergyPlus I/O variables to be exchanged at each time step are specified using a configuration file read by the BCVTB environment. Although EnergyPlus has the capacity to output a large number of variables, only a select few (zone 2 and outdoor environment conditions) are required in ensuring the external air conditions outside the different VCC components evolve in agreement with the weather and building conditions of the EnergyPlus model.

The cooling output from the VCC model is inputted into EnergyPlus using two separate

units which can supply either cooling or heating to perimeter zone 2. Specifying a negative energy load corresponds to the unit providing cooling. One unit is designated to supply only sensible cooling and the other unit is designated to supply only latent cooling. The sensible and latent cooling loads previously described are the loads sent to each unit. To ensure that no additional cooling is supplied to zone 2, the cooling coil in perimeter zone 2 was turned off.

3.3.3 Interfacing Issues

A drawback of the interface between the two clients is the method by which the variables are exchanged. Since the exchange of variables between MATLAB and EnergyPlus is accomplished in a single instance, there is an inherent delay between when the control action is generated and when it is implemented. Instead of reading the current conditions of the EnergyPlus building model, generating a control action in MATLAB and implementing this control, the interface uses a slightly different procedure. At the beginning of each time interval, the exchange function is called and the conditions of the building model at the start of the time interval are inputted into MATLAB. Concurrently, the control action generated during the previous time interval is implemented on the building model. Since there is no separation between when the BSD socket is read and when it is written, there is always a delay of one time step for any control action generated in MATLAB. To reduce the effects of this delay, the smallest allowable time increment of 60 seconds was used during all simulations. It is reasonable to assume that zone air dynamics evolve at a slower rate than the control implementation delay, resulting in the delay having a minimal effect on the performance of the VCC model.

During the initialization routine of the EnergyPlus model, problems in the synchronization of both clients at the start of the simulation period occur. EnergyPlus initializes the building model using weather data from the period immediately prior to the first day of the simulation period. Starting from an initial guess, the first day of the simulation is repeated until wall temperatures converge within a set tolerance. Following this initialization routine, the

EnergyPlus model is again initialized using the initial inputs from the VCC model (external interface). Due to the delay using the exchange function, this double initialization causes a discontinuity between the initial values of both simulation clients. As a result, minor fluctuations occur at the start of every simulation period. To avoid complications with the discontinuity at initialization, all simulations were run for 2 hours open loop at the nominal operating conditions, prior to implementing closed loop strategies on the VCC.

3.3.4 Model Predictive Control

One of the main contributions of this work was regulating a VCC using a model predictive control (MPC) approach. Before delving into the specific details of the MPC design, a general description of model predictive control is presented. A model predictive controller uses a process model to obtain a future input trajectory which causes the predicted output values to evolve in a manner which optimally satisfies a specific performance measure while ensuring input/output constraints are not violated. The time period which the input trajectory spans is known as the control horizon and the predicted output trajectory spans a time period known as the prediction horizon. The predictive controller obtains values for the inputs over the control horizon by solving an optimization problem which minimizes an objective function (usually defined in terms of the predicted output and input values over their respective horizons) by adjusting the decision variables of the problem, which are the input values. Once the input trajectory values are obtained, only the input values for the first predicted time step are implemented on the actual process, allowing for the current state/output values to update the initial conditions used in the next control calculation in the MPC controller. The initial conditions are continuously updated as the actual process evolves.

Chapter 4

Model Improvements and Control Design

This chapter outlines the improvements made to the original VCC model in addition to the formulation and implementation of both the classical and predictive control strategies on the interfaced VCC-building system.

4.1 Evaporator model with condensing capacity

For condensing conditions over the evaporator, an optimization problem is solved where the objective function is a rearrangement of the terms in the energy balance of the evaporator which contains terms associating energy with the wall, air and the water condensed on the outside of the evaporator. The energy balance is rearranged such that the difference between the term describing the heat tranfer from the evaporator wall to the air and the air enthalpy difference term is minimized. The objective function (J) is defined as in Equations 4.1 - 4.2, where the objective function is squared to ensure a minimal absolute value which ensures the conservation of energy is upheld. $T_{air,out}$ is the only decision variable in the objective function and is constrained to remain between 0 ^{o}C and 50 ^{o}C to ensure that

$T_{air,out}$ stays within a realistic range of values. The $T_{air,out}$ range was chosen loosely on the most extreme conditions which an air conditioning unit might be operated in. No detail was given in the original Thermosys toolbox as of why $T_{air,out}$ was obtained through solving an optimization problem rather than obtaining $T_{air,out}$ through solving the set of nonlinear equations using a common nonlinear solver, such as fsolve in MATLAB.

$$J = (\alpha_{o,e} A_{o,e} \sum_{i=1}^{2} \frac{L_{e,i}}{L_{e,Total}} (T_{air,avg} - T_{w,i}) - \Delta h)^2 \tag{4.1}$$

$$\begin{aligned} \Delta h = {} & \dot{m}_{dry\ air} C_{p,dry\ air} (T_{air,in} - T_{air,out}) + \dot{m}_{dry\ air} (w_{in} h_{in,water\ vap} - w_{out} h_{out,water\ vap}) \\ & - \dot{m}_{dry\ air} (w_{in} - w_{out}) C_{p,water} T_{air,out} \end{aligned} \tag{4.2}$$

Initially, $T_{air,out}$ is computed assuming no condensation occurs. If $T_{air,out} > T_{dp}$, then the assumption is correct. Otherwise, the condenstation method is invoked and $T_{air,out}$ is recalculated. If $T_{air,out} \leq T_{dp}$, then the condensation assumption is correct.

Once it is determined that the outlet air conditions are accurate, the latent and sensible cooling loads are calculated based on Equations 4.3 - 4.4, where the *Total Cooling Load* was equal to Δh as defined in Equation 4.2.

$$Latent\ Cooling\ Load = \dot{m}_{dry\ air} (w_{in} - w_{out}) \Delta h_{vl} \tag{4.3}$$

$$Sensible\ Cooling\ Load = Total\ Cooling\ Load - Latent\ Cooling\ Load \tag{4.4}$$

In Equation 4.3, Δh_{vl} is defined as the difference between the saturated water vapor enthalpy (h_v) and the saturated liquid water enthalpy (h_l) evaluated at the saturated vapor pressure corresponding to the average air temperature (T_{avg}) used in the evaporator energy balance calculations. If condensation does not occur, the latent cooling load is zero.

4.2 Evaporator condensation model correction

It is to be noted that the original Thermosys Simulink VCC model used an incorrect objective function in the condensing method. The energy balance originally did not accurately account for the enthalpy associated with the condensed water. In the corrected VCC model the enthalpy associated with the condensed water is represented by Equation 4.5 where the $m_{air}(w_{in}$ - $w_{out})$ represents the mass of water vapor which condenses.

$$h_{water,liquid} = \dot{m}_{dry\ air}(w_{in} - w_{out})C_{p,water}T_{air,out} \tag{4.5}$$

In the incorrect VCC model, the enthalpy associated with the condensed water was represented by Equation 4.6 which defines the enthalpy of the condensed water with an additional term to Equation 4.5, $\mathbf{\Delta h_{vl}}$. This is incorrect as the energy released when the water vapor condenses ($\mathbf{\Delta h_{vl}}$) is absorbed by the wall and accounted for in the heat transfer term between the air and wall in the incorrect objective function (same air-wall heat transfer term as in Equation 4.1)

$$h_{water,liquid} = \dot{m}_{dry\ air}(w_{in} - w_{out})C_{p,water}T_{air,out} + \mathbf{\Delta h_{vl}} \tag{4.6}$$

4.3 Conversion from Simulink to Matlab

The original Thermosys simulator was a simulink-based toolbox in MATLAB which called separate m-files corresponding to the static and ordinary differential equations (ODEs) defined earlier. Using a simulink interface slowed the completion time of simulations and complicated the procedure for implementing non-simulink control strategies on the VCC.

For these reasons, a m-file only VCC model was developed that had identical dynamics as the Thermosys VCC Simulink model.

The original Simulink VCC simulator modeled each component as an individual function where the outputs of one VCC component were the inputs of the next connected component (ie. expansion valve outputs would become inputs for pipe 1 in Figure 4.1). Using the Simulink model, adjusting the initial conditions of the VCC was more complex as seperate files were required to initialize the states of each dynamic components (heat exchangers and compressor).

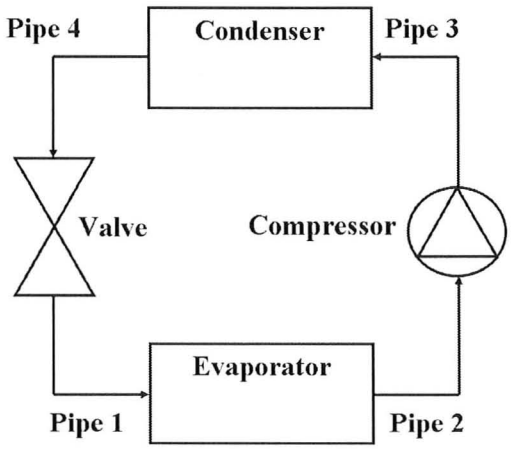

Figure 4.1: VCC Schematic

The m-file only VCC model is a function of only the integration time step, current state values, input values and ambient conditions. This function combines all the individual component m-files from the Simulink model, forming a function consisting of ODEs, static equations and lookup tables. Other static equations and lookup tables not previously described, are a part of the VCC model and required for determining various thermodynamics parameters as well as for populating the partial derivative terms in the heat exchanger ODEs. The output of this function is the $\dot{x}$ vector representing the dynamic states of the VCC in addition to a seperate vector consisting of non-state outputs values. The $\dot{x}$ vector is integrated over the given time step, to provide updated state values corresponding to the end time of the integration step. Using the m-file only VCC model allowed control strategies to be defined outside the main VCC function which used the current output and state measurement values as feedback for the calculation of subsequent control moves. The ambi-

ent conditions are defined outside the main VCC function, which allows for straightforward adjustments to be made to the ambient conditions. This was beneficial to the interfacing of the VCC model with the external software which provided time-varying ambient conditions.

The time-savings acheived is best expressed through a comparison of the execution time required to complete an open loop simulation of 1000 seconds operating the VCC at arbitrarily chosen operating conditions corresponding to a compressor RPM of 1100 and a valve opening of 11 % open. The execution time for both the simulink and m-file VCC models are presented in Table 4.1. The m-file based VCC was able to reduce the open loop simulation times by at least four times compared to the Simulink-based VCC model.

VCC Model	Execution Time (seconds)
Simulink	3476
M-file	840

Table 4.1: Open loop Simulation Times

4.4 Refrigerant mass flow rate correction

The VCC model being used assumes that the evaporator refrigerant outlet mass flow rate and condenser refrigerant inlet mass flow rate are equal to the refrigerant mass flow rate flowing through the compressor ($\dot{m}_k$). $\dot{m}_k$ is used with P_e and $h_{e,out}$ to define the pressure drop ΔP in pipe 2. $\dot{m}_k$ is used with P_c and $h_{k,out}$ to define ΔP in pipe 3. This also holds true on the opposite side of the VCC where the evaporator refrigerant inlet flow rate and the condenser refrigerant outlet flow rate are equal to the refrigerant mass flow rate defined by the expansion valve static equation (Equation 3.7) . ΔP in pipe 4 is dependent on $\dot{m}_v$, P_c and the condenser outlet refrigerant enthalpy $h_{c_{ro}}$. The ΔP in pipe 1 is dependent on $\dot{m}_v$, P_e and $h_{c_{ro}}$. All the ΔP calculations are in accordance with Equations 4.7 and 4.8.

$$\Delta P = \frac{L\dot{m}f}{2DA_{cs}\rho} \tag{4.7}$$

where L is the length of the pipe, D is the pipe diameter f is a friction factor based on the Reynolds Number, A_c is the cross-sectional area of the pipe and ρ is the density of the refrigerant.

$$\rho = f(h, P) \tag{4.8}$$

where P is the refrigerant pressure and h is the refrigerant enthalpy.

In the original Thermosys Simulink model, an initialized value of the refrigerant $\dot{m}$ was used to determine the ΔP in the different pipes without verifying that the calculated $\dot{m}$ (calculated from Equation 3.2 or 3.7) was accurate. The calculated $\dot{m}$ accuracy depends on the initialized $\dot{m}$ used in calculating ΔP, meaning if the $\dot{m}$ used in the ΔP calculation is not in agreement with the current states, the subsequent value of the calculated $\dot{m}$ and state variables could be inaccurate.

In ODE systems, static equations, such as the $\dot{m}$ equations (Equation 3.2 or 3.7), are dependent on only the current values of the state variables. In the original model, the calculated $\dot{m}$ was dependent on the previous and current values of the state variables because the initialized $\dot{m}$ value used in the ΔP calculation was calculated based on previous state variables. This calculation method is accurate if the system has reached steady-state, however for non-steady-state operating conditions the accuracy of the calculated $\dot{m}$ could be improved. To ensure that the initialized $\dot{m}$ used in the ΔP calculation is dependent on the current state variables, a tolerance on $\dot{m}$ is implemented on the static equations used to calculate the compressor and expansion valve $\dot{m}$. The tolerance compared the current and initialized values of $\dot{m}$, recalculating $\dot{m}$ if the difference between the current and initialized $\dot{m}$ was more than the specified tolerance. Once the difference between the current and initialized $\dot{m}$ is less or equal to the specified tolerance, it is concluded that the current $\dot{m}$ is

in agreement with the current state variables.

4.5 Flow Parameter values

The valve C_d lookup tables were only populated for $\Delta P > 1000$ kPa and the compressor efficiency (η) lookup tables were only populated for $2 \leq P_{ratio} \leq 6$. If either ΔP or P_{ratio} fell outside the lookup table bounds, no values were available for C_d or the η terms.

In [Eldredge and Alleyne [2006]], a mapping equation was fitted to the experimental values in the C_d lookup table. There was relatively no discrepancy between the predicted C_d values from the mapping equation and the experimental C_d values, which allowed the $\Delta P > 1000$ kPa constraint to be eliminated through replacing the C_d lookup table with the C_d mapping equation.

Mapping equations were also fit for the experimental values in the η lookup tables. However, there was a large discrepancy between the η mapping equation values and the experimental η values, resulting in the η values still being obtained from the lookup tables. To ensure η values existed outside the bounds of P_{ratio}, it was decided that if $P_{ratio} > 6$ or $P_{ratio} < 2$, the η terms would have a value corresponding to $\eta(P_{ratio} = 6)$ or $\eta(P_{ratio} = 2)$, respectively.

4.6 Rescaled VCC

The original VCC had a cooling capacity of 1127 watts the equivalent of a 0.32 ton cooling capacity. This cooling capacity was insufficient in regulating the supply air temperature between 22 - 24 ^{o}C for return and ambient air conditions associated with a common summer day. This motivated the rescaling of the VCC physical parameters.

Table 4.2 contains the original and rescaled values of all the adjusted physical parameters. Increasing the length of the evaporator (L_e) allows the medium being cooled, to be in

contact with the evaporator wall longer resulting in more heat removal. It was assumed as the length of the evaporator increases, the inner and outer areas of the evaporator ($A_{e,i}$, $A_{e,o}$) and the total mass of the evaporator ($Mass_e$) increase by the same factor as L_e. The diameter of the evaporator pipe (D_e) was also increased to allow for more heat transfer between the wall and the refrigerant. The air mass flow rate ($\dot{m}_{e,air}$) was increased allowing for more air flow over the evaporator.

Increasing the evaporator parameters caused an increase in the amount of heat absorbed by the refrigerant and to ensure this added heat could be dissipated to the ambient, the condenser parameters were increased. The same parameters were increased for the condenser and denoted with a subscript c. The refrigerant mass flow rate ($\dot{m}_{ref}$) as well as the compressor volume (V_k) were increased to allow for the refrigerant to absorb the additional heat.

Parameters	Original	Rescaled
Cooling Capacity (Tons of refrigeration)	0.32	0.85
L_e (m)	11.46	57.29
$A_{e,o}$ (m^2)	3.07	15.34
$A_{e,i}$ (m^2)	0.32	1.60
$Mass_e$ (kg)	1.5475	7.7375
D_e (m)	8.90 x 10^{-3}	3.57 x 10^{-2}
$\dot{m}_{e,a}$ (kg/s)	0.243	2.43
L_c (m)	10.7	53.5
$A_{c,o}$ (m^2)	2.79	13.97
$A_{c,i}$ (m^2)	0.28	1.38
$Mass_c$ (kg)	4.66	23.30
D_c (m)	8.10 x 10^{-3}	3.24 x 10^{-2}
$\dot{m}_r$ (kg/s)	7.764 x 10^{-3}	1.126 x 10^{-2}
V_k (m^3)	3.042 x 10^{-5}	1.521 x 10^{-4}

Table 4.2: Original and Rescaled VCC Physical Parameters

4.7 Nonlinear dynamics of VCC

To evaluate the nonlinearity in the VCC process, openloop step changes were implemented at different operating points. The output step responses were fitted with a First Order with Time Delay (FOTD) model to provide estimates for the gain and settling times corresponding to the specific operating points. The inputs of the VCC, compressor RPM and valve opening, were the step variables, and the output variables fitted with FOTD models were the evaporator superheat temperature (T_{SH}) and the evaporator supply air temperature (T_{SA}).

The compressor RPM step responses corresponded to an increase of 100 RPM (1500-1600 RPM) at different nominal valve values. The valve opening step responses corresponded to an increase of 1 % open (10-11 % open) at different nominal RPM values. Figures 4.2(a) and 4.2(b) display the gain and settling time values for the various operating points for T_{SA} responses to the RPM and valve step changes, respectively.

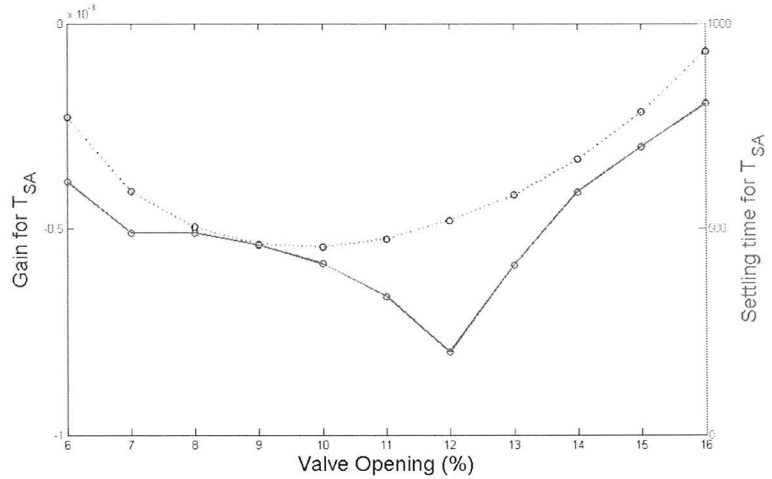

(a) T_{SA}-RPM

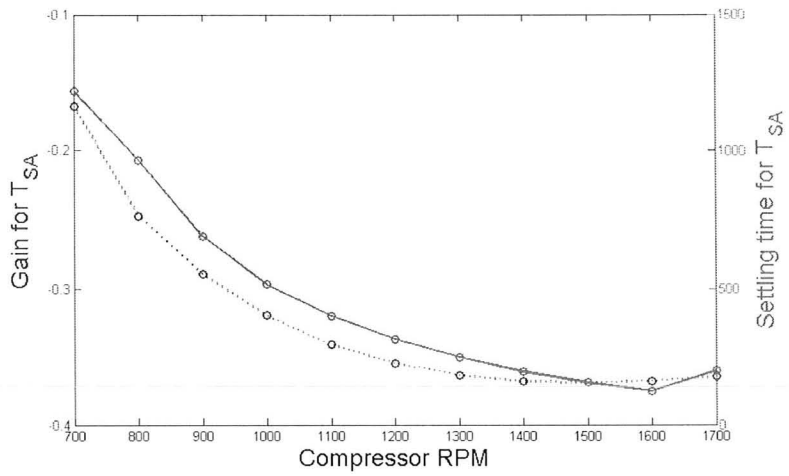

(b) T_{SA}-Valve

Figure 4.2: T_{SA} Gain/Settling Time values at Different Operating Points

Figures 4.3(a) and 4.3(b) display the gain and settling time values for the various operating points for T_{SH} responses to the RPM and valve step changes, respectively.

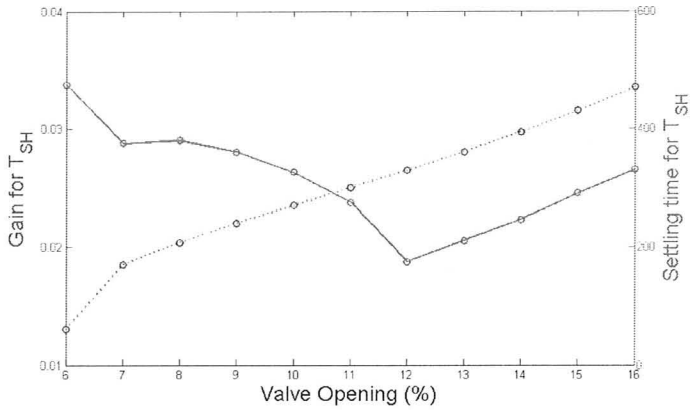

(a) T_{SH}-RPM

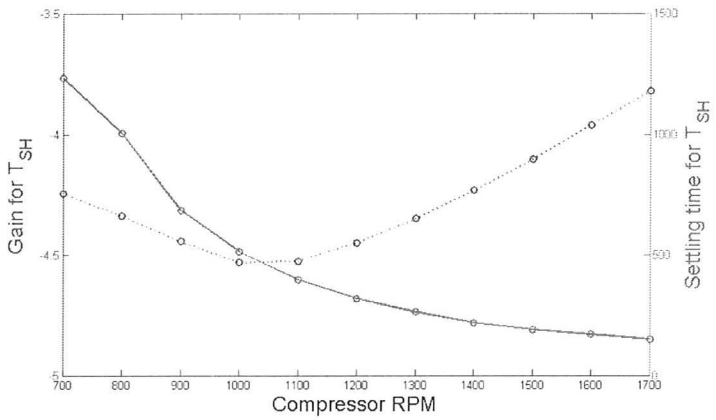

(b) T_{SH}-Valve

Figure 4.3: T_{SH} Gain/Settling Time values at Different Operating Points

The corresponding T_{SA} and T_{SH} responses to step changes in both RPM and valve opening are located in the Appendix.

It was observed that the gain and time constant vary significantly as the operating conditions are changed, indicating that the VCC is highly nonlinear. In [Rasmussen [2005]] a pattern for the gains of the evaporator output variables was observed for operating the experimental VCC at various operating points. It was determined that larger gains occur at operating points corresponding to lower compressor RPM and valve opening values. This trend was

attributed to larger magnitude changes in the refrigerant mass flow rate occurring at lower nominal operating points, resulting in larger changes in T_{SA} and T_{SH} for the evaporator air and refrigerant, respectively. This trend was present in the original Thermosys VCC, however in the modified VCC model, this gain pattern was not observed. Instead, at intermediate operating points, the T_{SA} and T_{SH} gains for different inputs would begin to increase as the nominal valve opening and/or compressor RPM increased. Through further investigation into the gain patterns of the VCC model, it was determined that at various intermediate operating points large changes in the magnitude of the refrigerant mass flow rate occurred, resulting in the experimental gain trend not being applicable to the simulated VCC. This gain discrepancy is likely due to a large variation in the VCC dynamics caused from the scaling-up of the individual VCC components, which caused the empirical parameters obtained from the experimental system (ie. C_d, η, etc.) to correspond to different VCC operating conditions. This could result in large gain fluctuations occurring at intermediate operating conditions if the values of the empirical parameters were larger.

4.8 Control of stand-alone VCC unit

Both classical and predictive control designs were initially implemented on the stand-alone VCC to determine if the regulating ability of a classical control design could be improved upon. The inlet air temperature and humidity outside both heat exchangers were held constant for the stand-alone VCC, allowing for the direct evaluation of each control strategy in terms of regulating the VCC outputs without being influenced by fluctuations in the air conditions. The performance of each control design was evaluated based on the ability to provide effective T_{SA} tracking of a SP trajectory which included both feasible and infeasible SP values, in addition to considering both T_{SH} and energy conservation effects which will be described in more depth in a later section. Infeasible SP values were included in the T_{SA} SP trajectory to ensure that the prescribed control action corresponded to operating the VCC at conditions which minimized the infeasibility (ie. VCC operating conditions which brought T_{SA} closest to infeasible SP). Also of interest was ensuring that each control

strategy would quickly and accurately prescribe control moves once the T_{SA} SP transitioned between an infeasible and feasible value.

By using a T_{SA} SP trajectory instead of various individual T_{SA} SP changes, this provided a reasonable approximation of the prescribed T_{SA} behaviour of regulating the interfaced VCC system with a cascade control structure which is the control design used for the interfaced system. By using a SP trajectory consisting of various desired T_{SA} values this ensured that the regulation of the VCC would be evaluated over a wide range of operating conditions. The values used in the T_{SA} SP trajectory were not chosen to ensure that the operating conditions for the stand-alone VCC corresponded exactly to the interfaced VCC system, but the SP values were chosen to correspond to a range of operating conditions that could occur through regulating the VCC of the interfaced system. Due to the similar nature in operating conditions, both the classical and predictive control designs were fine tuned based on their closed-loop performance in regulating the stand-alone VCC, prior to being implemented on the interfaced VCC system.

The classical PI and model predictive control structures on the stand-alone VCC are displayed in Figures 4.4 and 4.5, respectively.

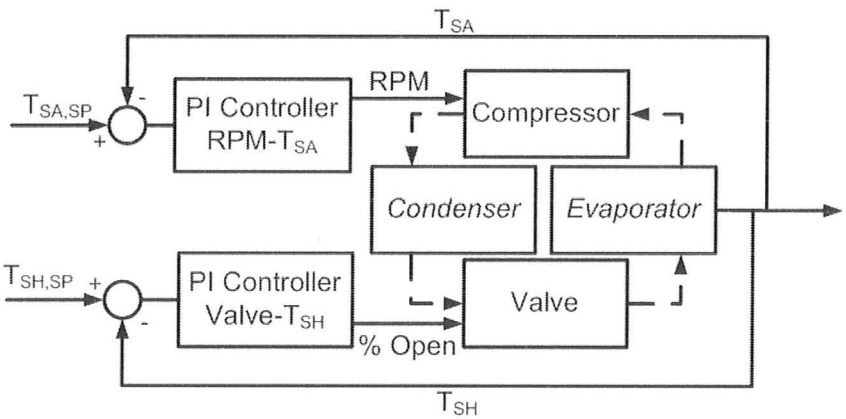

Figure 4.4: PI stand-alone Control Structure

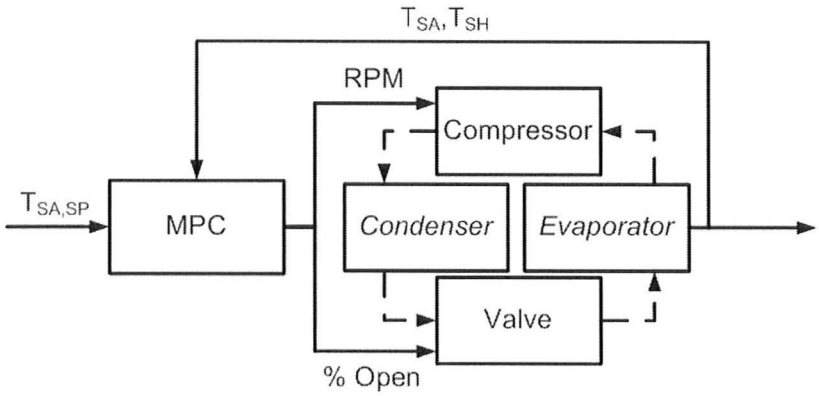

Figure 4.5: MPC Stand-alone Control Structure

4.9 Cascade Control Structure

The manipulated variables in the VCC model available for control are the compressor RPM and the expansion valve opening. In an actual VCC, the fan speeds for the air being blown over either heat exchanger are also available for adjustment, however in the VCC model the air mass flow rate over each heat exchanger is held constant.

Output variables relevant to common control objectives include the air temperature at the evaporator exit, which is referred to as the supply air temperature (T_{SA}) as well as the evaporator superheat temperature (T_{SH}). It is important to regulate T_{SA} because the energy associated with the supply air is the mechanism used by the VCC to provide cooling to a desired environment. Ensuring that no liquid enters the compressor is essential to reducing the wear in the compressor, specifically eliminating the potential damage to the cylinder and piston from attempting to compress liquid refrigerant. The T_{SH} should be maintained above 0 ^{o}C to ensure no liquid enters the compressor.

Prior to the control design, openloop step tests were performed on the compressor RPM and valve opening to gain an understanding of the VCC and interfaced system dynamics. The time constants (τ) for the T_{SA} and T_{SH} step responses with respect to the VCC inputs,

in addition to the time constant for the zone air temperature (T_{zone}) with respect to a step in T_{SA} are displayed in Table 4.3.

The operating conditions used for these tests corresponded to (compressor RPM, valve opening) of (1200 RPM, 10 % open). An individual step change of +100 RPM and a +1 % open were used for the τ calculations for the compressor and valve opening step responses, respectively. To identify τ between T_{SA}-T_{zone}, all internal loads and ambient conditions were held constant and the sensible cooling load was varied. By maintaining the building heat loads at constant values, the effect of a variation in the sensible cooling load and thus, a variation in T_{SA}, was directly observed for T_{zone}. A step change of -696 Watts corresponding to a T_{SA} step change of -1.35 ^{o}C was used for the sensible cooling load step size.

I/O Pair	τ (seconds)
RPM-T_{SA}	71
Valve-T_{SA}	563
RPM-T_{SH}	278
Valve-T_{SH}	73
T_{SA}-T_{zone}	2553

Table 4.3: Openloop Time constants for various I/O pairings of VCC-building system

It is evident that the VCC dynamics are considerably faster than the zone dynamics which motivated using a cascade control structure to regulate T_{zone}. The cascade control structure consisted of an inner loop in which T_{SA} and T_{SH} were regulated using the compressor RPM and expansion valve, which was then connected to an outer loop, responsible for regulating T_{zone} through adjusting the T_{SA} set point (SP) being presribed to the inner loop. The T_{SA} SP was updated every 22.5 minutes to ensure that the variation in T_{SA} would be captured in the T_{zone} dynamics. Through evaluating the performance of the PI and MPC strategies in conjunction with various T_{SA} SP updating times, the most effective value, in terms of at least one of the control methods being able to provide offset-free T_{SA} SP tracking, was determined to be 22.5 minutes.

The outer loop was controlled with a proportional-integral (PI) controller which used identical tuning parameters for cascade configurations consisting of either a linear MPC strategy or a classical PI strategy regulating the inner loop. By using an identical outer loop control strategy the performance of the inner control strategy with respect to regulating the VCC could be evaluated without bias from the outer loop control strategy. The tuning values used in the outer PI controller were chosen such that the T_{SA} SP values prescribed to the inner control strategy ensured that the Zone temperature conditions satisfied specific comfort standards (a more detailed explaination presented in Section 5.2).

4.10 Classical Control Design

The classical control strategy regulated T_{SA} and T_{SH} using individual PI controllers. To identify suitable I/O pairings for the controllers, openloop step tests were performed on the standalone VCC and a relative gain array (RGA) matrix was constructed as displayed in Equation 4.9. The first row corresponds to T_{SA} and the first column corresponds to RPM.

$$\begin{bmatrix} 0.195 & 0.805 \\ 0.805 & 0.195 \end{bmatrix} \tag{4.9}$$

From the RGA analysis, it would appear that the best I/O pairings would be RPM-T_{SH} and Valve Opening- T_{SA}, however it was decided based on common industrial practice of regulating T_{SH} with the expansion valve and also due to the openloop τ values for T_{SH} (Table 4.3), that RPM-T_{SA} and Valve Opening- T_{SH} would be the I/O pairings used. It was determined that increasing the physical dimensions of the individual components of the VCC caused the magntiude of the system dynamics to vary considerably from the original VCC model. This claim is supported through comparing the open-loop gain matrices for each of the scaled and original VCC model at an arbitrary operating point (1500 RPM, 10 % Open) as displayed in Equation 4.10-4.11.

$$\begin{bmatrix} -1.09 \text{ x } 10^{-3} & -0.22 \\ 2.58 \text{ x } 10^{-2} & -7.44 \end{bmatrix} \tag{4.10}$$

$$\begin{bmatrix} -1.46 \text{ x } 10^{-4} & -0.10 \\ 2.38 \text{ x } 10^{-2} & -3.95 \end{bmatrix} \tag{4.11}$$

The PI controllers were initialized with IMC (internal model control) tuning values and fine tuned using a manual iterative approach which emphasized minimizing the IAE (integral of absolute error) with respect to rejecting disturbances in the return/ambient air conditions. The T_{SA} SP value was prescribed by the outer PI controller and the T_{SH} SP was chosen at a value of 10 ^{o}C. Maintaining T_{SH} at a low value allows the VCC to absorb more heat because the length of the superheated region in the evaporator decreases, resulting in a longer two-phase region being able to absorb more heat. Using a T_{SH} SP lower than 10 ^{o}C caused worse T_{SA} SP tracking due to interaction between the multiple PI control loops.

The PI cascade control structure is displayed in Figure 4.6.

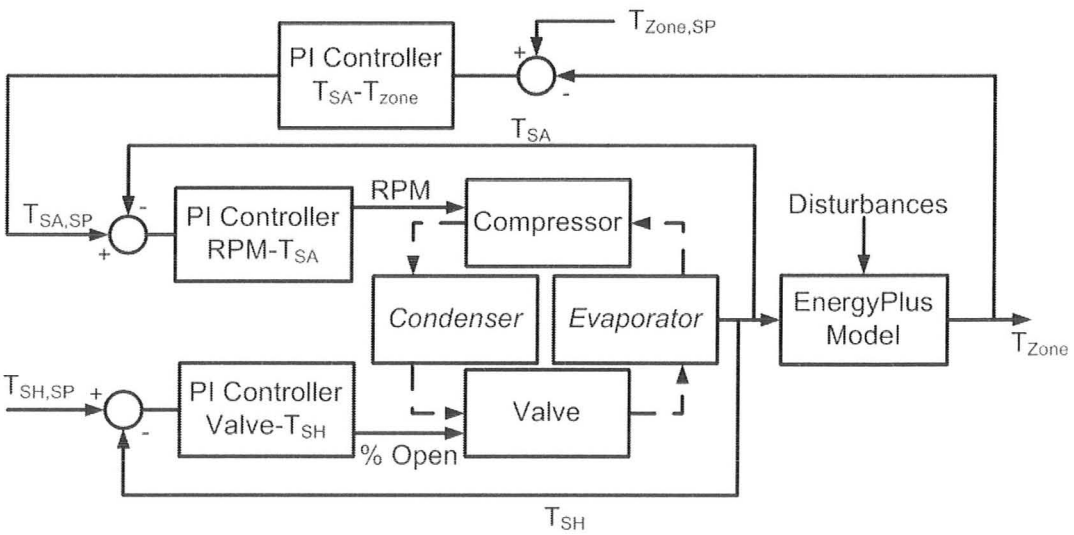

Figure 4.6: PI Cascade Control Structure

4.11 Model Predictive Control Design

The model predictive control (MPC) cascade control structure is displayed in Figure 4.7.

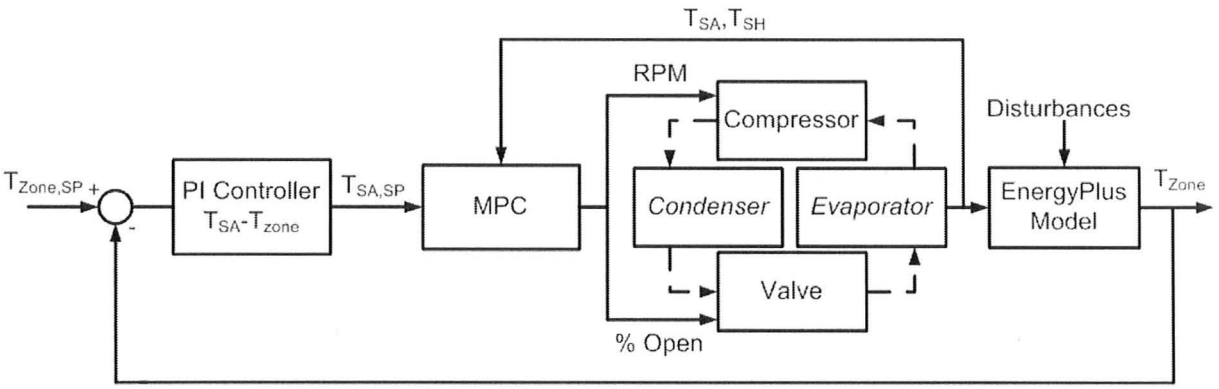

Figure 4.7: MPC Cascade Control Structure

In developing a model for the predictive control strategy, emphasis was placed on the following factors:

- Capturing the nonlinearity in the control variables of interest (T_{SA}, T_{SH}) due to:

  VCC dynamics

  Common load disturbances associated with the operation of a building

- Using a model identification procedure applicable to various cooling units, including units prior to installation as well as for pre-existing cooling units

Regulating the interfaced system using a MPC strategy with the same nonlinear VCC model would have accurately predicted the T_{SA} and T_{SH} values as the system dynamics would have been captured in the control action calculations resulting in minimal plant-model mismatch. However, deviations still would exist if this nonlinear MPC strategy was used to regulate the experimental VCC system as the varying ambient conditions would

not be captured in the VCC model, in addition to plant-model mismatch occurring from the nonlinear model being an approximation of the actual dynamics of the experimental system. As the experimental VCC system was a scaled version of an industrial VCC, the magnitude of the plant-model mismatch would increase considerably between this nonlinear model and an actual VCC system, reducing the benefit of using such a detailed dynamic model in the MPC calculations.

Using a model obtained through the linearization of the nonlinear VCC model at a specific operating point also has significant drawbacks for the regulation of either an actual VCC or the nonlinear VCC model. Obtaining a linear state space model about a specific operating point would only capture the local dynamics of the VCC, which includes only a small neighborhood of operating conditions. Operating the actual VCC outside this relatively small operating region would cause the plant-model mismatch to increase considerably as supported by the analysis performed in Section 4.7 on the nonlinearity of the VCC. The added benefit of being able to monitor both output and state variables is not essential to the regulation of a VCC, as the system stability is related directly to T_{SH} and the cooling capacity of the VCC is related directly to T_{SA}. However, in the case of fault detection, it may be advantageous to use a model which predicts both measurable output and state variables as it could provide faster detection and corrective action.

From an industrial perspective, it's important to capture the T_{SA} and T_{SH} dynamics for any cooling unit which can include, but is not restricted to, VCC systems. As there are various types of cooling units in production, in addition to unique modifications made to pre-existing cooling units, it's essential to use a model structure and identification procedure which can account for the individuality of the cooling unit. This motivated the use of individual autoregressive exogenous (ARX) models to capture the T_{SA} and T_{SH} dynamics. The identification procedure used to obtain relevant system data for model formulation follows.

4.11.1 Model Identification Procedure

After interfacing the VCC model with the Energyplus building model, it was determined that not only did the compressor RPM and valve opening position (VO) significantly affect the T_{SA} and T_{SH} dynamics, but also the return air temperature (T_{return}) and the ambient air temperature (T_{amb}) caused considerable variations in the VCC dynamics. This motivated using an identification procedure which captured variations in not only the VCC manipulated variables, but also in the air conditions outside both heat exchangers (T_{return} outside the evaporator, T_{amb} outside the condenser).

Pseudo random binary sequences (PRBS) were implemented for each of RPM, VO, T_{return} and T_{amb} on the standalone VCC in order to capture the individual and combined effect of these variables on T_{SA} and T_{SH}. The PRBS were designed to capture the entire operating range of the VCC in terms of RPM and VO values as well as to capture a common range of return and ambient air conditions experienced on a typical summer day in a building. Individual ARX models were fit to the T_{SA} and T_{SH} PRBS responses. The PRBS variables and the T_{SA} and T_{SH} actual and ARX model responses are displayed in Figure 4.8.

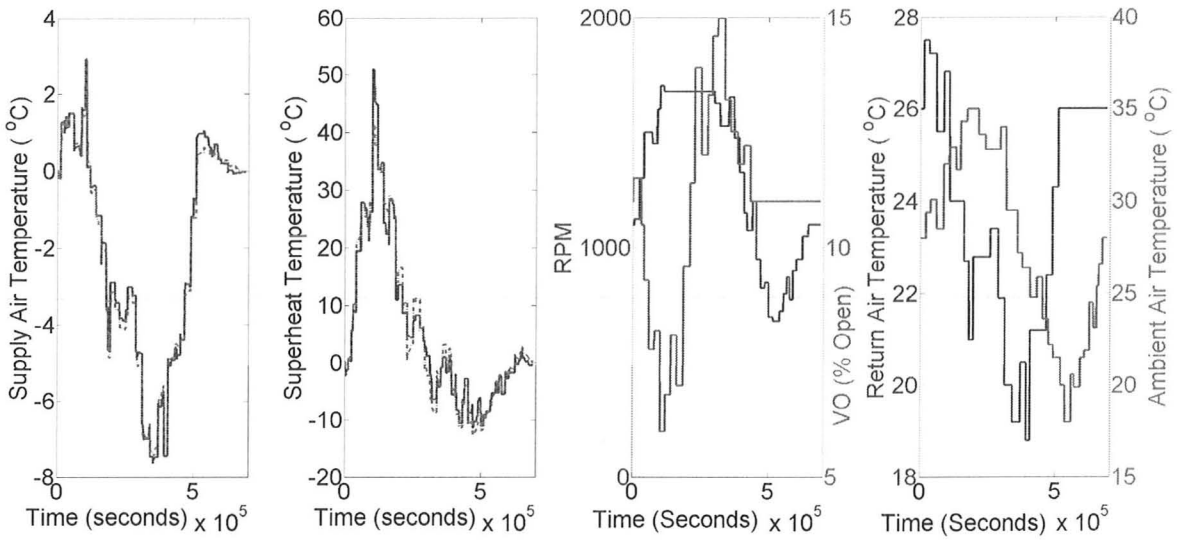

Figure 4.8: PRBS data used for ARX Model Identification (– – Model response, – Actual response)

The ARX models are of the form of Equation 4.12. The ARX coefficients were obtained using the System Identification toolbox which solves a least squares optimization problem as described by Equation 4.13. The number of lags used in each ARX model were determined through comparing the qualitative fit of each ARX model with the actual output response for various lag combinations. The lag combinations which had the best qualitative fit for each ARX model are located in Table 4.4.

$$\begin{aligned} Y_i(k) = {} & a_1 Y_1(k-1) + \ldots a_{N_a} Y_1(k-N_a) + b_1 Y_2(k-1) + \ldots b_{N_b} Y_2(k-N_b) \\ & + c_1 U_1(k-1) + \ldots c_{N_c} U_1(k-N_c) + d_1 U_2(k-1) + \ldots d_{N_d} U_2(k-N_d) \\ & + e_1 Z_1(k-1) + \ldots e_{N_e} Z_1(k-N_e) + f_1 Z_2(k-1) + \ldots f_{N_f} Z_2(k-N_f) \end{aligned} \tag{4.12}$$

where Y_1 corresponds to T_{SA}, Y_2 is T_{SH}, U_1 is RPM, U_2 is VO, Z_1 is T_{amb} and Z_2 is T_{return}

$$\min_{\mathbf{a_1 \ldots f_{N_f}}} \sum_{i=1}^{N_{total}} Y_{actual,i} - Y_{model,i} \tag{4.13}$$

where N_{total} represents the number of data points used in the regression.

ARX Model	N_a	N_b	N_c	N_d	N_e	N_f
T_{SA}	1	1	1	1	1	1
T_{SH}	2	2	2	2	2	2

Table 4.4: Lags of ARX models

4.11.2 Optimization Problem Formulation

In this formulation the prediction and control horizons were equivalent and denoted as N_c in the below MPC formulation.

$$\min_{\mathbf{u}_i} \sum_{i=1}^{N_c} (\hat{y}_{2,i} - y_2^{\mathrm{SP}*})^{\mathrm{T}} \mathbf{Q}_2 (\hat{y}_{2,i} - y_2^{\mathrm{SP}*}) + (\hat{y}_{1,i} - 3.5)^{\mathrm{T}} \mathbf{Q}_1 (\hat{y}_{1,i} - 3.5) + u_1^{\mathrm{T}} \mathbf{R}_1 u_1 + \Delta u_2^{\mathrm{T}} \mathbf{R_{d2}} \Delta u_2 + \Delta u_1^{\mathrm{T}} \mathbf{R_{d1}} \Delta u_1 \tag{4.14}$$

subject to: (4.15)

$$3.5^{\circ}\mathrm{C} - \alpha_{1,low} + \beta_{1,low} \leq \hat{y}_{1,i} \leq 20^{\circ}\mathrm{C} - \alpha_{1,up} + \beta_{1,up} \tag{4.16}$$

$$\mathbf{u}_{\min} \leq \mathbf{u}_i \leq \mathbf{u}_{\max} \tag{4.17}$$

$$\Delta \mathbf{u}_{\min} \leq \Delta \mathbf{u}_i \leq \Delta \mathbf{u}_{\max} \tag{4.18}$$

where $\hat{y}_i(k) = a_1 y_1(k-1) + \ldots f_{N_f} z_2(k - N_f)$, (4.19)

$$y_2^{\mathrm{SP}*} = y_2^{\mathrm{SP}} - \alpha_2 + \beta_2, \tag{4.20}$$

$$\alpha_{\mathbf{j}} = \frac{\mathbf{y_j(0)} - \hat{\mathbf{y}}_{\mathbf{j}}\mathbf{(0)}}{\mathbf{\Gamma_j}} \; \forall \, j = 1, 2, \tag{4.21}$$

$$\beta_2 = \frac{\Delta t(y_2^{\mathrm{SP}} - y_2(0))}{\Lambda_2} + \beta_2, \tag{4.22}$$

$$\beta_{1,low} = \begin{cases} \frac{\Delta t(3.5 - y_1(0))}{\Lambda_{1,low}} + \beta_{1,low} & : y_1(0) < 3.5 \\ 0 & : y_1(0) \geq 3.5, \end{cases} \tag{4.23}$$

$$\beta_{1,up} = \begin{cases} \frac{\Delta t(20 - y_1(0))}{\Lambda_{1,up}} + \beta_{1,up} & : y_1(0) > 20 \\ 0 & : y_1(0) \leq 20 \end{cases} \tag{4.24}$$

Important control objectives which must be considered when regulating a VCC include:

- Providing effective T_{SA} tracking
- Maintaining T_{SH} at a minimal value
- Operating the VCC using minimal RPM

The air temperature of the environment being cooled will evolve based on a variety of factors related to the cooling unit. These include the quantity of air conditioned in a single pass through the VCC, the VCC cooling capacity and the ability of the VCC to provide effective T_{SA} SP tracking. The former two factors are physical characteristics of the VCC, however the latter factor is dependent on the VCC control structure. By providing effective T_{SA} SP tracking this allows the environment air temperature to reach it's desired setting in the least amount of time.

T_{SA} SP tracking was incorporated in the optimization formulation by penalizing the deviation of the predicted T_{SA} from its SP value over the prediction horizon using a quadratic term in the objective function (Equation 4.14). The T_{SH} values over the prediction horizon were kept at low values by bounding each T_{SH} value in the prediction horizon between 3.5^{o}C and 20^{o}C (Equation 4.16). To further ensure the prescribed control action corresponded to a low T_{SH} value, a quadratic term which penalized the deviation of T_{SH} from it's lower bound was added to the objective function. As mentioned earlier, operating the VCC at low T_{SH} values allows for more heat absorption, resulting in the VCC being more energy efficient.

Operating the VCC with minimal RPM, reduces the power consumed by the VCC, saving the user money and reducing the VCC ecological footprint. To minimize the RPM, the objective function was penalized using a quadratic term which penalized the absolute value of RPM (Equation 4.14). The experimental VCC system used in constructing the VCC model was only valid for a specific range of RPM and VO operating conditions. To ensure the RPM and VO values over the control horizon were within the valid operating range, the

RPM and VO values were bounded between the upper and lower values of the experimental operating range (Equation 4.17). To reduce wear on the mechanical components in the compressor and valve the difference between successive control action moves was constrained between an upper and lower bound (Equation 4.18).

To account for plant-model mismatch an error term (α_i) was subtracted from the T_{SA} SP and from the lower and upper T_{SH} bounds. The error term was defined as the difference between the predicted output value from the previous control calculation and the current observed output value (Equation 4.21). Subtracting α_i shifts the T_{SA} SP and T_{SH} bounds, used in the optimization problem, in a manner in which the prescribed control action causes the actual T_{SA} to move closer to T_{SA} SP. Shifting the SP and bounds in the controller only by the α_i values does not guarantee that the prescribed control action will acheive offset-free tracking as the T_{SA} SP inside the controller only incorporates the difference between the predicted and observed T_{SA} values without correcting for the difference between T_{SA} and its respective SP. The α_i was not added to the prediction values because for prediction horizons greater than one time step in length, the error between the actual and predicted values will vary from the α_i value due to accumulation of this α_i term in the ARX model. This accumulation effect is caused by the dependence of the current ARX model output on the previous predicted output values.

To account for the actual T_{SA} SP deviation a β_i term was added to the T_{SA} SP used in the optimization problem. This β_i term is defined as the sum of the T_{SA} SP error, resulting in T_{SA} SP in the controller to continually adjust until the actual T_{SA} reaches its SP. As the actual T_{SA} approaches its desired SP, the change between successive β_i terms will decrease, operating in a similar manner as the integral mode of a PI controller when the CV approaches its SP.

During certain intervals of the test period, the plant-model mismatch was larger due to sudden changes in the internal gains and/or ambient conditions (ie. transitioning between intervals of schedules or slow changes in the air temperature). During these intervals the prescribed valve and RPM movement oscillated between the upper and lower Δu bounds

to account for the oscillating nature of the plant-model mismatch. By adding quadratic Δu terms in the objective function, which penalized excessive valve and RPM movement, it was observed that the oscillations during the intervals of large-plant model mismatch reduced, in addition to smoothing out the valve and RPM movement over the entire test period (Equation 4.14).

The specific values for the constraints and tuning parameters in the MPC formulation are located in Table 4.5.

Parameters	N_c	$\mathbf{Q}_2$	$\mathbf{Q}_1$	$\mathbf{R}_1$	$\mathbf{R}_{d2}$	$\mathbf{R}_{d1}$	$\mathbf{\Lambda_2}$	$\mathbf{\Lambda_{1,low}}$	$\mathbf{\Lambda_{1,up}}$	$\mathbf{\Gamma_2}$	$\mathbf{\Gamma_{1,low}}$	$\mathbf{\Gamma_{1,up}}$	$\mathbf{u}_{\min}$	$\mathbf{u}_{\max}$	$\Delta\mathbf{u}_{\min}$	$\Delta\mathbf{u}_{\max}$
Value	4	2000	0.12	$\frac{10}{1700^2}$	0.002	1	100	70	400	5	50	10	$\begin{bmatrix}678.8 & 6\end{bmatrix}$	$\begin{bmatrix}1700 & 15\end{bmatrix}$	$\begin{bmatrix}-200 & -1\end{bmatrix}$	$\begin{bmatrix}200 & 1\end{bmatrix}$

Table 4.5: MPC Parameter values

4.11.3 Achieving Offset-free Tracking

To better understand the effect of each correcting factor used in adjusting the SP and bounds of the optimization problem, closed-loop simulations were completed with and without the aforementioned correcting factors active and the T_{SA} responses were compared.

Initially, a MPC design without any correcting factors was used to regulate the stand-alone VCC. There was considerable offset observed between the actual T_{SA} and its SP caused by the plant-model mismatch due to the discrepancy between the ARX model and the actual nonlinear VCC model. The next step was to account for the plant-model mismatch using the α_i term which acted as a dynamic correcting factor that would capture the variation between plant and model as the operating conditions changed. The final adjustment to the MPC design was adding the β_i term to T_{SA} SP to incorporate corrective action in the optimization problem corresponding to the actual T_{SA} SP error.

The T_{SA} responses for each MPC design are displayed in Figure 4.9. It is to be noted that the T_{SA} response corresponding to the MPC design using only the α_i correcting term corresponded to the same MPC tuning parameters as located in Table 4.5, except the $\mathbf{\Gamma_2}$ value was set to 1 to provide a more aggressive adjusting factor.

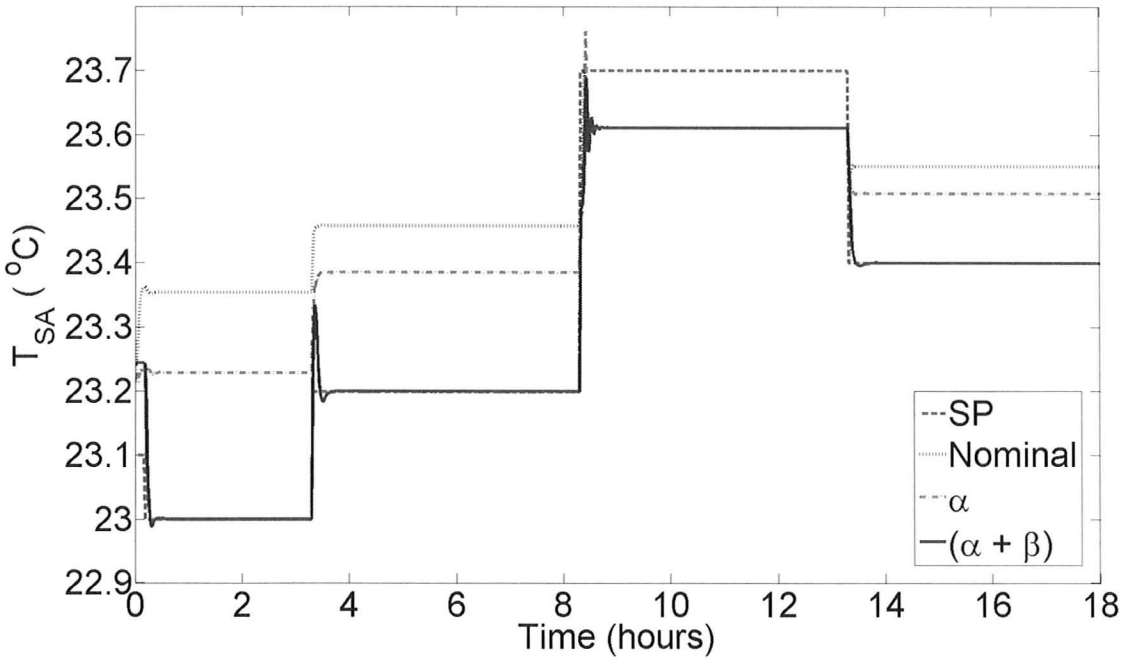

Figure 4.9: T_{SA} responses of different MPC designs

Chapter 5

Results

This chapter begins with describing the test conditions and closed-loop results of the stand-alone VCC followed by a full description of the same aspects of the interfaced VCC. This includes details wth regards to the ambient air conditions, closed-loop performance criteria and the closed-loop trajectories of each control strategy.

5.1 Stand-alone VCC

The stand-alone VCC inlet air conditions were chosen to correspond to arbitrary summer conditions and were maintained at the constant values summarized in Table 5.1 for the entire test period. The air conditions over the evaporator were selected such that condensation would occur during the test period.

Air Parameter	Value
T_{amb} (^{o}C)	28
T_{return} (^{o}C)	26
RH (%)	0.87

Table 5.1: Stand-alone VCC Air Conditions

The closed-loop performance for each control strategy was evaluated using measures to quantify the T_{SA} SP tracking performance for a SP trajectory spanning a time period of 1090 minutes (18 hours and 10 minutes). These measures included a nonstandard T_{SA} integral of absolute error (IAE) measure as defined by Equation 5.1 and a measure which summed the individual T_{SA} settling times (within $\pm$ 2.5 % of steady-state) for the different SP changes in the SP trajectory. The PI control strategy used a T_{SH} SP of 10 ^{o}C with the varying T_{SA} SP trajectory.

$$IAE = \Delta t \sum_{i=1}^{1090} \frac{[T_{SA}SP(i) - T_{SA}(i)]^2}{T_{SA}SP(i)} \tag{5.1}$$

where Δt is the time step used in the integration of the interfaced system (60 seconds).

Also of importance when evaluating the closed-loop performance is the energy efficiency of the VCC. A large portion of the energy consumed by the VCC can be contributed to the energy used through operating the compressor. This motivated using the summation of the instantaneous compressor power ($\omega_{instant}$) over the test period,as given in Equations 5.2 - 5.3, as an approximation for the VCC energy demand .

$$\omega_{instant} = \frac{\dot{m}_k(h_{out} - h_{in})}{\eta_k} \tag{5.2}$$

$$Total\,Power = \Delta t \sum_{i=1}^{1090} \omega_{instant,i} \tag{5.3}$$

Figure 5.1 displays the closed-loop VCC input/output variable responses for both the PI and MPC strategies and Table 5.2 contains the values of the performance measures.

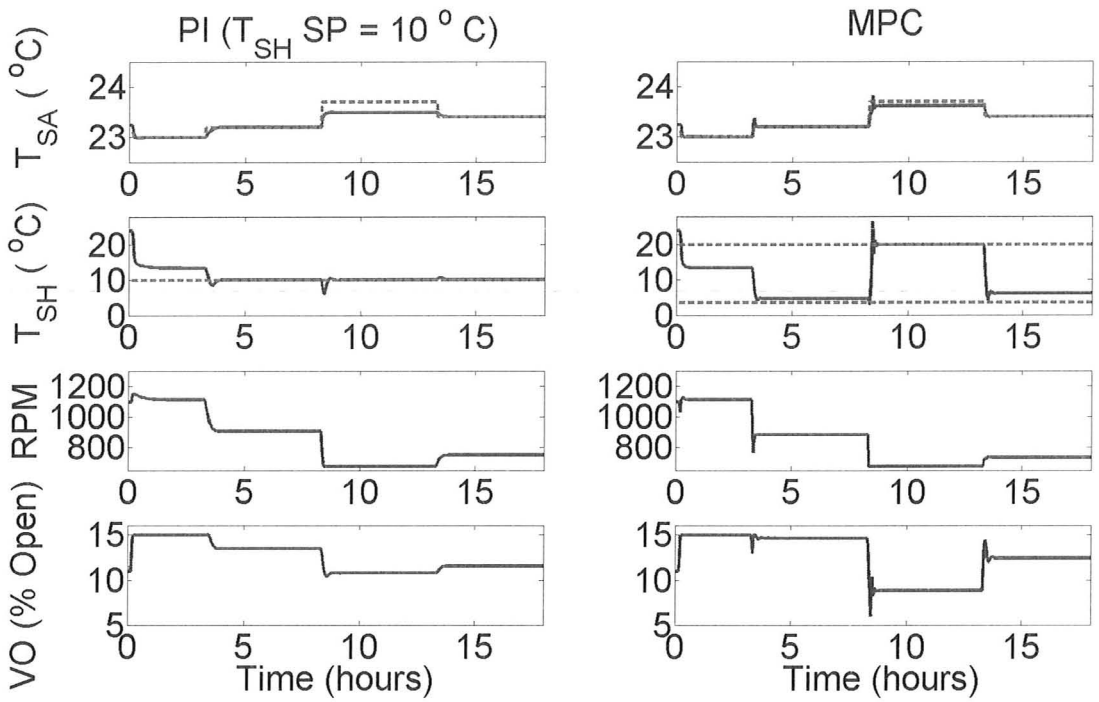

Figure 5.1: Closed-loop I/O variable responses for stand-alone VCC (-- SP, – Actual response)

Control Structure	PI(T_{SH} SP= 10 ^{o}C)	MPC
T_{SA} IAE (s·^{o}C)	35.32	7.64
T_{SA} Cumulative Settling Time (seconds)	6120 (1800 1800 900 1620)	2880 (420 480 1140 840)
Cumulative Power (kJ)	10017	9222

Table 5.2: Stand-alone VCC Closed-loop Performance Measures

As evident from the closed-loop responses, the MPC strategy was able to provide offset-free tracking for various T_{SA} SP changes with faster settling times for each feasible SP value relative to the PI strategy. Due to the benefit of the predicitve controller in prescribing control moves corresponding to maintaining T_{SH} within a range of values, rather than a specific SP, the MPC strategy was able to provide more accurate tracking than the PI

strategy. This was evident for the infeasible T_{SA} SP as the MPC prescribed control action corresponded to T_{SH} being maintained at it's upper bound, which allowed the difference between the infeasible T_{SA} SP and the actual T_{SA} to be as small as possible. For the same T_{SA} SP, the PI control strategy required T_{SH} to be maintained at 10 ^{o}C which caused the T_{SA} SP error to be larger. The MPC strategy was able to use approximately 8 % less power over the test period due to the predictive controller being able to take advantage of the multi-variable nature of the VCC. This allowed the prescribed control moves to emphasize operating the VCC at high valve opening values instead of high RPM values for the various feasible SP values.

A further investigation into using the upper bound value from the MPC strategy (20 ^{o}C) for the T_{SH} SP in the PI control strategy was completed and the closed-loop VCC input/output variable responses are displayed in Figure 5.2 and Table 5.3 contains the values of the performance measures.

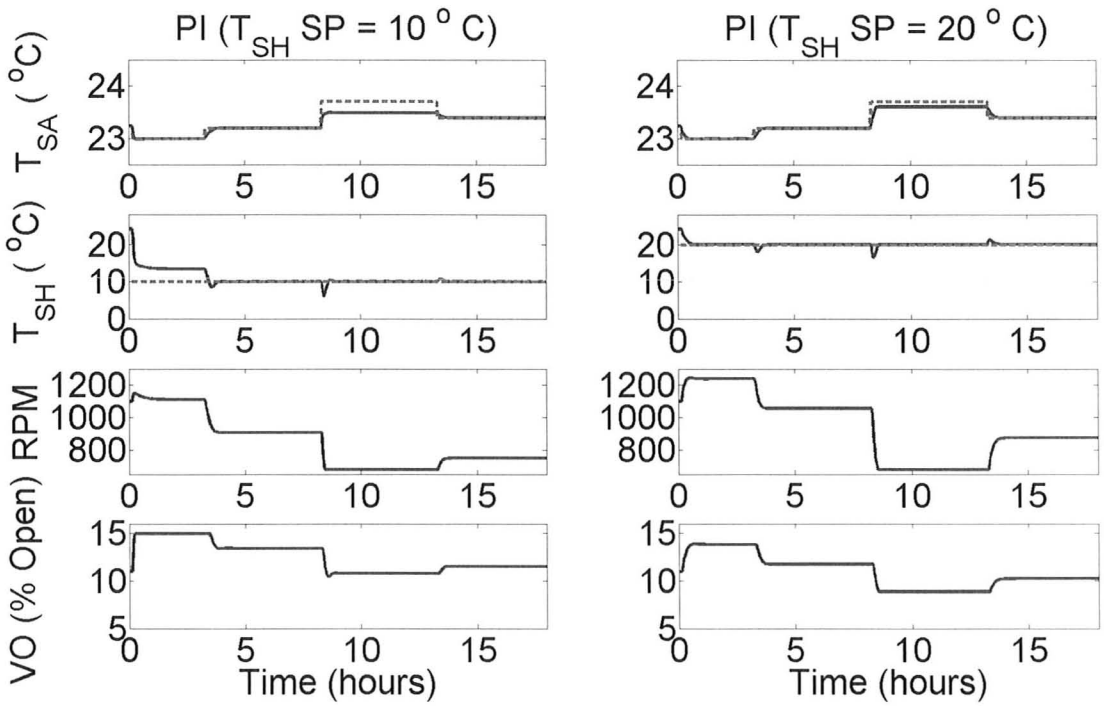

Figure 5.2: PI Closed-loop I/O variable responses for the stand-alone VCC (— SP, – Actual response)

Control Structure	PI(T_{SH} SP= 10 ^{o}C)	PI(T_{SH} SP= 20 ^{o}C)
T_{SA} IAE (s·^{o}C)	35.32	10.40
T_{SA} Cumulative Settling Time (seconds)	6120 (1800 1800 900 1620)	5520 (1140 1500 900 1980)
Cumulative Power (kJ)	10017	11915

Table 5.3: Stand-alone VCC PI Performance Measures

By maintaining T_{SH} at 20 ^{o}C, the PI control strategy was able to provide similar tracking ability as the MPC strategy for the infeasible T_{SA} SP value as evident by the lower T_{SA} IAE value. However, maintaining T_{SH} at a higher value, requires the valve opening to be operated at a lower nominal value, resulting in higher RPM values being prescribed by the T_{SA} -RPM controller to ensure T_{SA} tracked the various feasible SP values. This increase in compressor RPM is captured in the larger cumulative power value for the PI control strategy using a T_{SH} SP of 20 ^{o}C.

5.2 Interfaced VCC System

The interfaced system weather conditions corresponded to a common July day at the O'Hare Airport in Chicago with building internal gains common to a typical week day between 8:00 and 18:00. The internal gains capture heat variations caused by a variety of realistic heat loads such as the movement of people, lighting schedules and solar radiation. As the air in zone 2 is exposed to these internal gains, varying amounts of heat transfer occur as the amount of heat associated with the internal gains vary. This causes fluctuations in the temperature and humidity of the air in zone 2 and act as disturbances for the return air being supplied to the primary unit.

Figure 5.3 displays T_{amb} and the relative humidity (RH) of the ambient air and Figure 5.4 displays the variation in the internal gains for the test period.

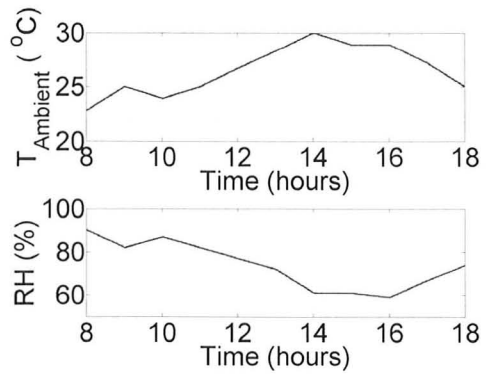

Figure 5.3: Interfaced System Ambient Air Conditions

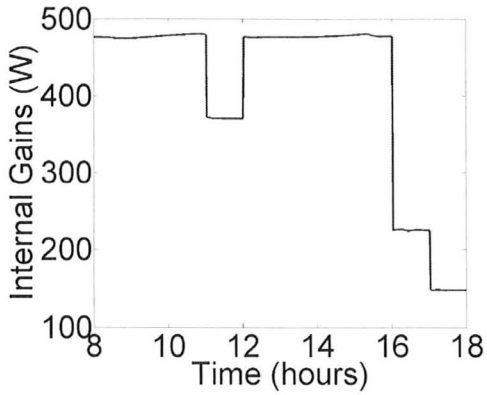

Figure 5.4: Interfaced System Internal Gain Conditions

Each control strategy was evaluated based on their ability to reject disturbances in T_{amb} and T_{return} while maintaining the T_{zone} within acceptable comfort standards. According to the American Society of Heating, Refrigeration and Air-Conditioning Engineers (ASHRAE), an acceptible air temperature in terms of comfort, is between 22 and 24 ^{o}C which motivated the use of a T_{zone} SP of 24 ^{o}C. Another important ASHRAE comfort standard is that T_{zone} should not vary outside a $\pm$ 0.5 ^{o}C band of T_{zone} SP for longer than 15 minutes or the human body will detect this temperature variation.

By ensuring T_{zone} satisfied the ASHRAE standards this resulted in a meaningful T_{SA} SP

being presribed to the inner loop VCC controller. The performance of the inner loop controller in terms of T_{SA} SP tracking was quantified using the same IAE term as defined in Equation 5.1 and the VCC energy demand was approximated using the aforementioned compressor power equations (Equations 5.2 - 5.3) over the test period (600 minutes, 10 hours).

Figure 5.5 displays the closed-loop VCC input/output variable responses for both the PI and MPC strategies. The MPC was able to lower T_{SH} closer to 0 ^{o}C due to the T_{SH} constraints contained in the optimization formulation. By maintaining T_{SH} at a lower value, better T_{SA} SP tracking was obtained using less power (lower RPM). From the openloop step tests performed in Section 4.7, insight can be gained into understanding the control action prescribed by the model predictive controller.

Lower T_{SH} values correspond to operating at a higher VO or operating at lower compressor RPM. Lower T_{SA} values correspond to higher VO or operating at higher compressor RPM. Due to penalizing the absolute value of the compressor RPM and the absolute value of T_{SH} in the objective function, the prescribed MPC action emphasizes operating at minimal RPM values and large VO values to maintain the T_{SH} close to it's lower bound value of 3.5 ^{o}C.

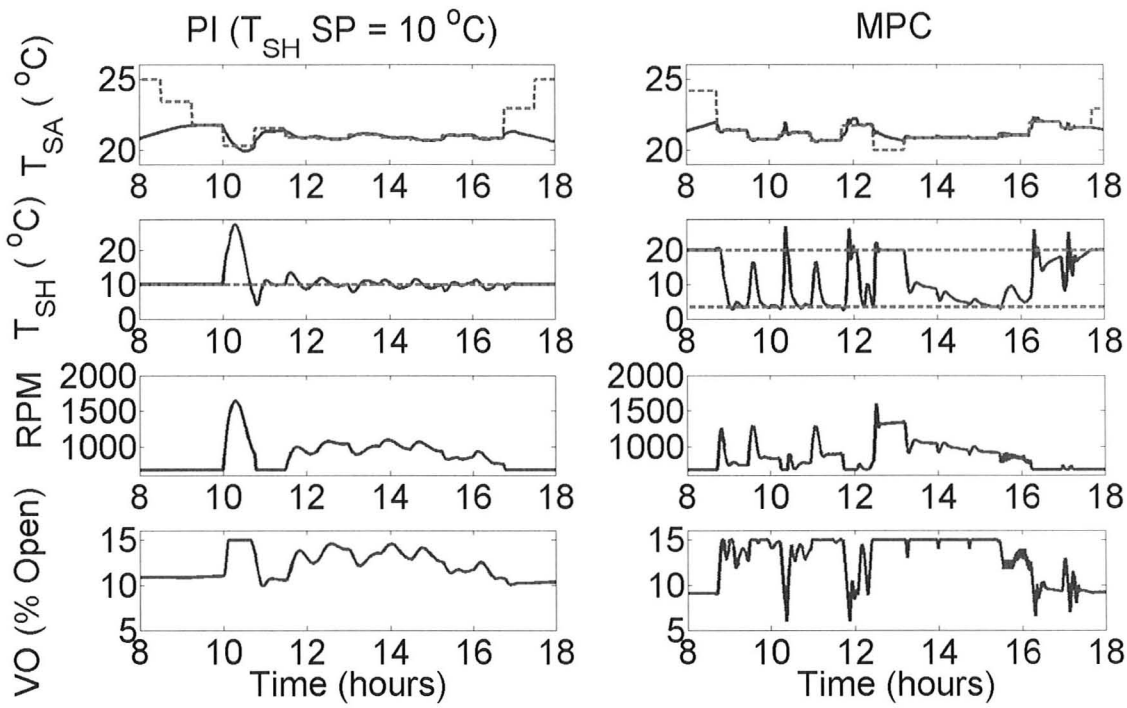

Figure 5.5: Closed-loop VCC I/O variable responses for Interfaced system (– – SP, – Actual response)

The MPC strategy was able to provide offset-free tracking for the majority of the T_{SA} SP values prescribed by the outer PI controller where as the classical control strategy was only able to bring T_{SA} within a neighborhood of the SP value, resulting in the classical control strategy being unable to provide offset-free tracking for the majority of its T_{SA} SP values. Figure 5.6 displays a zoomed view of the T_{SA} trajectories of Figure 5.5, which along with the value of the IAE measure presented in Table 5.4 support the offset-free tracking claim for the proposed MPC design. A small energy savings was obtained with the MPC strategy with respect to operating the compressor, however if the energy efficiency of the entire VCC is taken into consideration, the MPC strategy is able to operate the VCC much more effectively than the classical control strategy. This is evident from the closed-loop T_{SH} trajectories where the MPC strategy is able to maintain T_{SH} at it's lower bound for the majority of the test period whereas the classical control strategy maintains T_{SH} at it's

predefined SP for the majority of the test period. Further investigation into using a lower T_{SH} SP value in the classical control strategy was attempted, however T_{SH} SP less than 10 ^{o}C caused the superheat region in the evaporator to go to zero, causing a termination flag in the simulation.

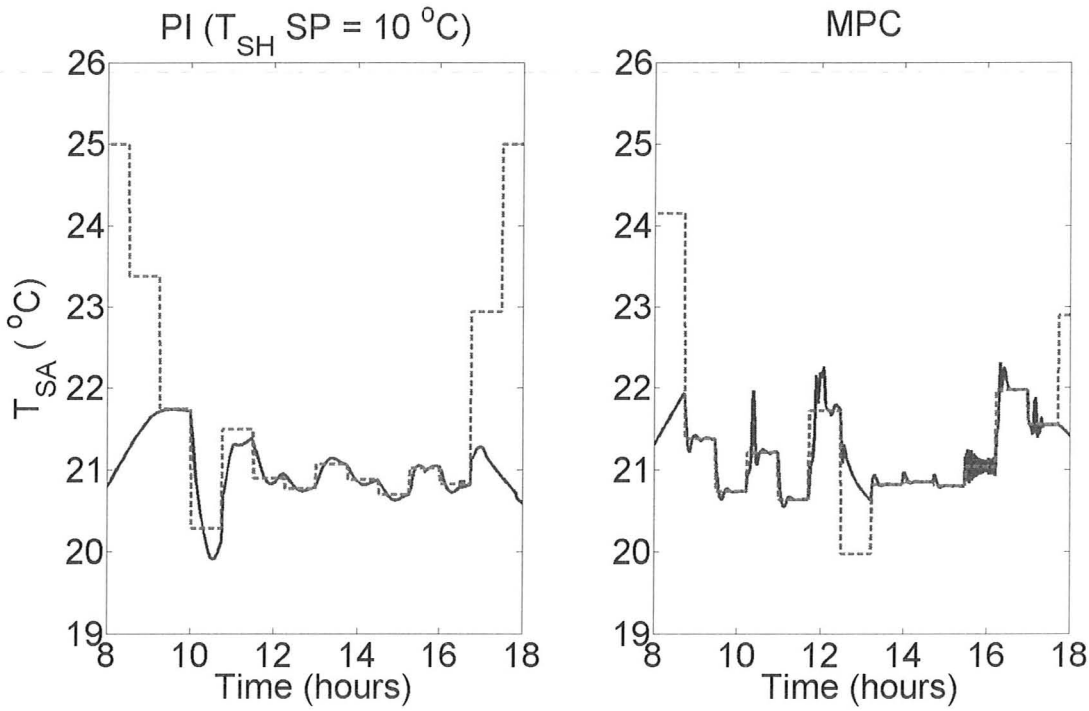

Figure 5.6: Closed-loop VCC T_{SA} responses for Interfaced system (– – SP, — Actual response)

The corresponding T_{zone} responses for each control strategy are located in Figure 5.7. The MPC strategy was able to maintian T_{zone} within ASHRAE standards for the entire test period whereas the PI strategy was not able to maintain T_{zone} within the ASHRAE standards. The T_{zone} violations of the upper bound value using the model predictive control strategy were less than 15 minutes, resulting in the ASHRAE standards still being satisified. Approximately the last 40 minutes of the test period corresponded to T_{zone} violating the ASHRAE standards when the VCC was being regulated using the PI control strategy.

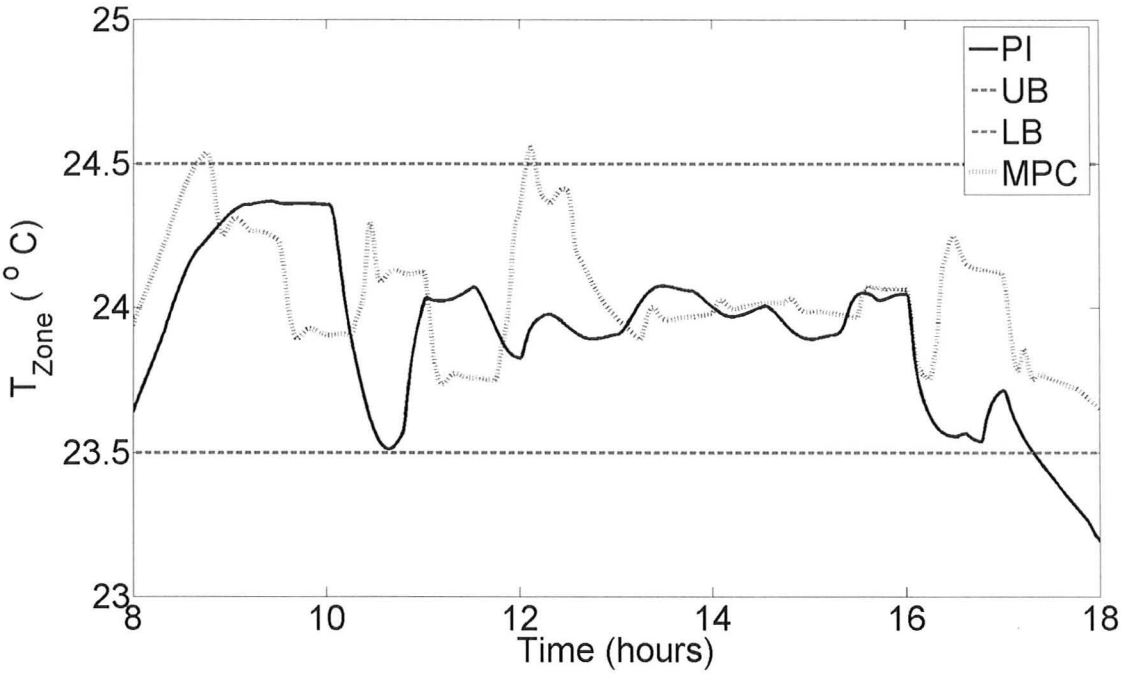

Figure 5.7: Closed-loop VCC T_{zone} response for each control strategy

The performance measure values for the PI and the MPC strategies are located in Table 5.4, where it was observed that a significant improvement was achieved by regulating the VCC using the MPC strategy in terms of T_{SA} SP tracking as well as reducing the energy demand of the VCC.

Control Structure	PI(T_{SH} SP= 10 ^{o}C)	MPC
Cumulative Power (kJ)	5763	5648
T_{SA} IAE (s·^{o}C)	3315	958

Table 5.4: Closed-loop Performance Measures

Chapter 6

Conclusions and Recommendations

6.1 Conclusions

In this work, control strategies were implemented on a detailed VCC model which contained realistic return and ambient air conditions provided through the interfacing of the VCC model with an EnergyPlus building model. This provided a detailed model for the zone air temperature dynamics, which incorporated a variety of realistic zone disturbances, specifically considering the effect of the conditioned air from an actual cooling unit in addition to common weather and internal load variations.

A cascade control structure was used to regulate the zone air conditions in the building model. The cascade structure was designed such that the outer loop regulated the zone air temperature through adjusting the set point of the VCC supply air temperature using a PI controller. The inner loop regulated the VCC supply air and superheat temperatures through adjustments to the compressor RPM and valve opening using a linear model predictive controller.

An ARX-based linear model predictive controller with disturbance rejection ability was used to regulate the VCC and it was determined that the predictive controller used less energy (reduction by 2.0 %) to provide better supply air tracking (a 71.1 % reduction

compared to PI). This was achieved through the incorporation of the multi-variable nature of the problem into the linear models and through the constraint handling abilities of MPC. By implementing superheat constraints, the MPC strategy was able to operate with the superheat closer to zero, resulting in better energy efficiency.

This work establishes the possibility of acheiving better energy efficiency by using MPC strategies for the control of energy systems.

6.2 Recommendations for Future Work

Further avenues to explore include forming a linear model based on clustering the operating points using a fuzzy c-means method to attempt to account for the varying dynamics between local operating regions in the VCC. Through a similar openloop identification procedure as used in this work, local linear models will be obtained for the interfaced system, which will more accurately model the local dynamics of the current operating conditions. The local linear models will be identified offline allowing for less computationally intensive calculations in the online MPC control action. As the current operating conditions change, this proposed linear-MPC design will adjust the linear model used in the MPC calculation by calculating the position of the current operating point relative to the operating regions used in the offline formulation of the various local linear models. If the current operating point falls into multiple operating regions, a weighted linear model will be formed based on the proximity of the current operating point to each of the overlapping operating regions of the different linear models. By forming a weighted linear model this eliminates any potential discontinuities which could arise from jumping between models during the prediciton stage in the model predictive controller.

Possible improvements to the current control structure could include modifying the outer loop control strategy to more accurately capture the effect of the supply air temperature on the zone air temperature which would allow for more relevant supply air set point values to be prescribed to the inner model predictive controller. Instead of using a PI controller, a

separate model predictive controller could be designed based on identifying an ARX model for the zone air temperature which accounts for variations in the supply air temperature, the internal gains and the ambient air temperature. By identifying the individual and combined effect of variations in these three factors (supply air temperature, internal gains, ambient air temperature) which cause the largest variation in the zone air conditions, the zone air dynamics could more accurately be identified and thus, regulated.

The regulation of the VCC could also be improved through introducing more variables for adjustment into the VCC model. This includes using a non-constant model for the air mass flow rate used for the air flowing over each heat exchanger, which incorporates the effect of adjusting the fan power on the air mass flow rate. By having a variable-speed fan model the energy consumed by the VCC would more accurately be represented. Incorporating a variable-speed fan into the VCC model would more accurately represents a large-scale cooling unit due to the fact that usually the non-conditioned (ie. return air) and conditioned air flow rates are regulated through duct work. Investigating the regulation of a primary unit, such as a chiller network, which directly cools a non-air medium (ie. water) would also be relevant to large-scale cooling units.

List of References

Alleyne, A., Keir, M., Hencey, B., Bin, L., and Jain, N. (2009). Decentralized Feedback Structures of a Vapor Compression Cycle System. *IEEE Transactiosn on Control Systems Technology*, .

Behidj, N., Brugger, M., Demers, D., Kowal, A., Liu, Y., Warbanski, M., and Yamada, F. (2009). Energy Efficiency Trends in Canada. In *Natural Resources Canada*, pp. 1–54.

Chen, Q., Worden, K., Peng, P., and Leung, A. (2007). Genetic algorithm with an improved fitness function for (N)ARX modelling. *Mechanical Systems and Signal Processing*, **21**, 994–1007.

Crawley, D. B., Lawrie, L. K., Winkelmann, F. C., Buhl, W. F., Huang, Y. J., Pedersen, C. O., Strand, R. K., Liesen, R. J., Fisher, D. E., Witte, M. J., and Glazer, J. (2001). EnergyPlus: creating a new-generation building energy simulation program. *Energy and Buildings*, **33**, 319–331.

Deru, M., Griffith, B., and Torcellini, P. (2006). Establishing Benchmarks for DOE Commercial Building R & D and Program Evaluation. In *ACEEE summer study on energy efficiency in buildings*, Vol. 1–12.

Eldredge, B. and Alleyne, A. (2006). Improving the Accuracy and Scope of Control-Oriented Vapor Compression Cycle System Models. *University of Illinois at Urbana-Champaign Dissertation*, , 1–121.

Garcia, C., Prett, D., and Morari, M. (1989). Model Predictive Control: Theory and Practice-a Survey. *Automatica*, **25**, 335–348.

Grieve, D. and Hughes, N. (2010). Reciprocating Compressors. In *School of Marine Science and Engineering. The University of Plymouth, Plymouth, United Kingdom.*

Harnischmacher, G. and Marqardt, W. (2007). Nonlinear model predictive control of multivariable processes using block-structured models. *Control Engineering Practice*, **15**, 1238–1256.

Huang, G., Wang, S., and Xu, X. (2009). A robust model predictive control strategy for improving the control performance of air-conditioning systems. *Energy Conversion and Management*, **50**, 2650–2658.

India (2007). HVAC and Refrigeration System. In *Bureau of Energy Efficiency. Government of India.*

Jain, N., Li, B., Keir, M., Hencey, B., and Alleyne, A. (2010). Decentralized Feedback Structures of a Vapor Compression Cycle System. *IEEE Transactions on Control System Technology*, **18**, 185–193.

Keir, M. and Alleyne, A. (2007). Feedback Structures for Vapor Compression Cycle Systems. *American Control Conference*, .

Leducq, D., Guilpart, J., and Trystram, G. (2006). Non-linear predictive control of a vapour compression cycle. *International Journal of Refrigeration*, **29**, 761–772.

Li, T. and Georgakis, C. (2008). Dynamic Input Signal Design for the identification of constrained systems. *Journal of Process Control*, **18**, 332–346.

Lin, J. and Yeh, T. (2002). Bond-graph modeling of the air-conditioning system. *Fourth Asian Control Conference*, , 1608–1613.

Lin, J. and Yeh, T. (2007). Modeling, identification and control of air-conditioning systems. *International Journal of Refrigeration*, **30**, 209–220.

MA, J., QIN, J. S., AND SALSBURY, T. (2010a). Real-Time Model Predictive Control for Energy and Demand Optimization of Multi-Zone Buildings . In *2010 AIChE Conference*.

MA, Y., BORRELLI, F., HENCEY, B., COFFEY, B., BENGEA, S., AND HAVES, P. (2010b). Model Predictive Control for the Operation of Building Cooling Systems. In *American Control Conference*, pp. 5106–5111.

MAEDER, U., BORRELLI, F., AND MORARI, M. (2009). Linear off-set free Model Predictive Control. *Automatica*, **45**, 2214–2222.

MAHMOOD, M. AND MHASKAR, P. (2008). Enhanced Stability Regions for Model Predictive Control of Nonlinear Process Systems. *AIChE J.*, **54**, 1487–1498.

MAY-OSTENDORP, P., HENZE, G. P., CORBIN, C. D., RAJAGOPALAN, B., AND FELSMANN, C. (2010). Model-predictive control of mixed-mode buildings with rule extraction. *Building and Environment*, , 1–10.

MAYNE, D., RAWLINGS, J., RAO, C., AND SCOKAERT, P. (2000). Constrained model predictive control: Stability and optimality. *Automatica*, **36**, 789–814.

MHASKAR, P. (2006). Robust model predictive control design for Fault-Tolerant Control of Process Systems. *Industrial & Engineering Chemistry Research*, **45**, 8565–8574.

MHASKAR, P. AND KENNEDY, A. (2008). Robust model predictive control of nonlinear process systems: Handling rate constraints. *Chemical Engineering Science*, **63**, 366–375.

MOROSAN, P., BOURDAIS, R., DUMUR, D., AND BUISSON, J. (2010). Distributed Model Predictive Control for Building Temperature Regulation. In *American Control Conference*, pp. 3174–3179.

MUSKE, K. AND BADGWELL, T. (2002). Disturbance Modeling for Offset-free Linear Model Predictive Control. *Journal of Process Control*, **12**, 617–632.

PANNOCHIA, G. AND RAWLINGS, J. (2003). Disturbance models for offset-free model predictive control. *AIChE Journal*, **49**, 426–437.

Rake, H. (1980). Step Response and Frequency Response Methods. *Automatica*, **16**, 519–526.

Rasmussen, B. (2005). Dynamic Modeling and Advanced Control of Air Conditioning and Refrigeration System. *University of Illinois at Urbana-Champaign Dissertation*, , 1–290.

Rivera, D., Lee, H., Mittelmann, H., and Braun, M. (2009). Constrained multisine input signals for plant-friendly identification of chemical process systems. *Journal of Process Control*, **19**, 623–635.

Sandipan, M., Alleyne, A., and Chandan, V. (2010). Predictive Control of Complex Hydronic Systems. In *American Control Conference*, pp. 5112–5117.

Sarabia, D., Capraro, F., Larsen, L., and Prada, C. (2007). Hybrid Control of a Supermarket Refrigeration System. In *American Control Conference*, pp. 4178–4185.

Schurt, L., Hermes, C., and Neto, A. (2009). A model-driven multivariable controller for vapor compression refrigeration systems. *International Journal of Refrigeration*, **32**, 1672–1682.

Wetter, M. and Haves, P. (2008). A Modular Building Controls Virtual Test Bed for the Integration of Heterogeneous Systems. In *3rd National Conference of IBPSA-USA*, pp. 69–76.

Xi, X., Poo, A., and Chou, S. (2007). Support vector regression model predictive control on a HVAC plant. *Control Engineering Practice*, **15**, 897–908.

Xu, M., Li, S., Cai, W., and Lu, L. (2006). Effects of a GPC-PID control strategy with hierarchical structure for a cooling coil unit. *Energy Conversion and Management*, **47**, 132–145.

Yuan, Z. and L., L. (1985). Unprejudiced Optimal Open Loop Input Design for Identification of Transfer Functions. *Automatica*, **21**, 697–708.

Zhu, G., Henson, M., and Megan, L. (2001). Dynamic modeling and linear model predictive control of gas pipeline networks. *Journal of Process Control*, **11**, 129–148.

Appendix

A Conversion of PDEs to ODEs

The fundamental conservation PDEs used to describe the energy and mass balances of each heat exchanger (Equations 3.9-3.11) were converted to ODEs and then subsequently to the matrix form of Equation 3.12, by integration using the Leibniz's rule (Equation 6.1).

$$\int_{z_1(t)}^{z_2(t)} \frac{\partial f(z,t)}{\partial t} dz = \frac{d}{dt}\left[\int_{z_1(t)}^{z_2(t)} f(z,t)dz\right] - f(z_2(t),t)\frac{d(z_2(t))}{dt} + f(z_1(t),t)\frac{d(z_1(t))}{dt} \quad (6.1)$$

A detailed step by step procedure used to convert the mass, wall-refrigerant energy and air-wall energy PDEs to their respective ODEs is presented below in Equations **??-??**. Note z_1 is the horizontal position in the evaporator where the two-phase region contacts the superheat region.

Evaporator Two-Phase Mass Balance PDE conversion to ODE

$$\frac{\partial(\rho A_{cs})}{\partial t} + \frac{\partial \dot{m}}{\partial z} = 0 \quad (6.2)$$

$$\int_0^{L_{e,1}} \frac{\partial(\rho_{r,e1} A_{cs})}{\partial t} dz + \int_0^{L_{e,1}} \frac{\partial \dot{m}}{\partial z} dz = 0 \quad (6.3)$$

$$\frac{d}{dt}\left[\int_0^{L_{e,1}} \rho_{r,e1} A_{e,cs} dz\right] - \rho_{r,g} A_{e,cs} \dot{L}_{e,1} + 0 + \dot{m}_{r,e,int1} - \dot{m}_{r,e,in} = 0 \tag{6.4}$$

$$\frac{d}{dt}\left[\rho_{r,e1} A_{e,cs} L_{e,1}\right] - \rho_{r,g} A_{e,cs} \dot{L}_{e,1} = \dot{m}_{r,e,in} - \dot{m}_{r,e,int1} \tag{6.5}$$

$$\rho_{r,e1} = \bar{\gamma}\rho_{r,g} + (1-\bar{\gamma})\rho_{r,l} \tag{6.6}$$

$$A_{e,cs} L_{e,1}\left[\frac{d\rho_{r,l}}{dP_e}(1-\bar{\gamma}) + \frac{d\rho_{r,v}}{dP_e}\bar{\gamma}\right]\dot{P}_e + \left[\bar{\gamma}\rho_{r,g} + (1-\bar{\gamma})\rho_{r,l}\right] A_{e,cs}\dot{L}_{e,1} - \rho_{r,g} A_{e,cs}\dot{L}_{e,1} = \dot{m}_{r,e,in} - \dot{m}_{r,e,int1} \tag{6.7}$$

$$\left[\frac{d\rho_{r,l}}{dP_e}(1-\bar{\gamma}) + \frac{d\rho_{r,v}}{dP_e}\bar{\gamma}\right] A_{e,cs} L_{e,1}\dot{P}_e + (\rho_{r,l} - \rho_{r,g})(1-\bar{\gamma}) A_{e,cs}\dot{L}_{e,1} = \dot{m}_{r,e,in} - \dot{m}_{r,e,int1} \tag{6.8}$$

Evaporator Two-Phase Refrigerant Energy Balance PDE conversion to ODE

$$\frac{\partial(\rho A_c h - A_c P)}{\partial t} + \frac{\partial(\dot{m}h)}{\partial z} = p_i \alpha_i (T_w - T_r) \tag{6.9}$$

$$\int_0^{L_{e,1}} \frac{\partial(\rho_{r,e1} A_{e,cs} h_{r,e1} - A_{e,cs} P_e)}{\partial t} dz + \int_0^{L_{e,1}} \frac{\partial(\dot{m}h)}{\partial z} dz = \int_0^{L_{e,1}} p_{i,e}\alpha_{i,e}(T_{e,w1} - T_{e,r1}) dz \tag{6.10}$$

$$\frac{d}{dt}\left[\int_0^{L_{e,1}}(\rho_{r,e1}A_{e,cs}h_{r,e1}-A_{e,cs}P_e)dz\right]-(\rho_{r,e1}A_{e,cs}h_{r,e1}-A_{e,cs}P_e)\dot{L}_{e,1}+\dot{m}_{r,e,int1}h_{r,v}-\dot{m}_{r,e,in}h_{r,e,in}$$
$$=L_{e,1}p_{i,e}\alpha_{i,e}(T_{e,w1}-T_{e,r1}) \tag{6.11}$$

$$A_{i,e}=L_{e,Total}\ \ p_{i,e} \tag{6.12}$$

$$\frac{d}{dt}(\rho_{r,e1}h_{r,e1}A_{e,cs}P_e)-\frac{d}{dt}(A_{e,cs}P_eL_{e,1})-(\rho_{r,e1}A_{e,cs}h_{r,e1}-A_{e,cs}P_e)\dot{L}_{e,1}+\dot{m}_{r,e,int1}h_{r,v}-\dot{m}_{r,e,in}h_{r,e,in}$$
$$=\frac{L_{e,1}}{L_{e,Total}}A_{i,e}\alpha_{i,e}(T_{e,w1}-T_{e,r1}) \tag{6.13}$$

$$\frac{d(\rho_{r,e1}h_{r,e1})}{dt}+\rho_{r,e1}h_{r,e1}A_{e,cs}\dot{L}_{e,1}-A_{e,cs}L_{e,1}\dot{P}_e-A_{e,cs}P_e\dot{L}_{e,1}-(\rho_{r,e1}A_{e,cs}h_{r,e1}-A_{e,cs}P_e)\dot{L}_{e,1}$$
$$=\dot{m}_{r,e,in}h_{r,e,in}-\dot{m}_{r,e,int1}h_{r,v}\frac{L_{e,1}}{L_{e,Total}}A_{i,e}\alpha_{i,e}(T_{e,w1}-T_{e,r1}) \tag{6.14}$$

$$\rho_{r,e1}h_{r,e1}=\bar{\gamma}\rho_{r,g}\,h_{r,v}+(1-\bar{\gamma})\rho_{r,l}\,h_{r,l} \tag{6.15}$$

$$\left[\frac{d(\rho_{r,l}h_{r,l})}{dP_e}(1-\bar{\gamma})+\frac{d(\rho_{r,v}h_{r,v})}{dP_e}\bar{\gamma}-1\right]A_{e,cs}L_{e,1}\dot{P}_e+(\rho_{r,l}h_{r,l}-\rho_{r,v}h_{r,v})(1-\bar{\gamma})A_{e,cs}\dot{L}_{e,1}$$
$$=\dot{m}_{r,e,in}h_{r,e,in}-\dot{m}_{r,e,int1}h_{r,v}+\alpha_{i,e,1}A_{i,e}\frac{L_{e,1}}{L_{e,Total}}(T_{e,w1}-T_{e,r1}) \tag{6.16}$$

Evaporator Two-Phase Wall Energy Balance ODE conversion

$$(C_p \rho A)_w \frac{\partial T_w}{\partial t} = p_i \alpha_i (T_r - T_w) + p_o \alpha_o (T_a - T_w) \tag{6.17}$$

$$\int_0^{L_{e,1}} (C_p \rho A)_w \frac{\partial T_w}{\partial t} dz = \int_0^{L_{e,1}} p_i \alpha_i (T_r - T_w) + p_o \alpha_o (T_a - T_w) dz \tag{6.18}$$

$$V_w = L_{e,1} \;\; A_w \tag{6.19}$$

$$(C_p \rho V)_w \dot{T}_{e,w1} = \alpha_{o,e} A_{o,e} (T_{a,e,avg} - T_{e,w1}) - \alpha_{i,e,1} A_{i,e} (T_{e,w1} - T_{e,r1}) \tag{6.20}$$

For brevity, this detailed procedure was only presented for the PDEs describing the two-phase region in the Evaporator. This same procedure was used to form the fundamental conservation ODEs for each fluid region in the different heat exchangers. The conservation ODEs corresponding to the evaporator and condenser are presented in Equations 6.21-6.26 and Equations 6.27 -6.35, respectively. [Rasmussen [2005]].

Evaporator Conservation of Refrigerant Mass (Two-Phase and Superheat Regions)

$$\left[\frac{d\rho_{r,l}}{dP_e}(1 - \bar{\gamma}) + \frac{d\rho_{r,v}}{dP_e} \bar{\gamma} \right] A_{e,cs} L_{e,1} \dot{P}_e + (\rho_{r,l} - \rho_{r,v})(1 - \bar{\gamma}) A_{e,cs} \dot{L}_{e,1} = \dot{m}_{r,e,in} - \dot{m}_{r,e,int1} \tag{6.21}$$

$$\left[\left. \frac{\partial \rho_{r,e2}}{\partial P_e} \right|_{h_{r,e2}} + \frac{1}{2} \left. \frac{\partial \rho_{r,e2}}{\partial h_{r,e2}} \right|_{P_e} \frac{dh_{r,v}}{dP_e} \right] A_{e,cs} L_{e,2} \dot{P}_e + \frac{1}{2} \left. \frac{\partial \rho_{r,e2}}{\partial h_{r,e2}} \right|_{P_e} A_{e,cs} L_{e,2} \dot{h}_{r,e,out} + (\rho_{r,v} - \rho_{r,e2}) A_{e,cs} \dot{L}_{e,1}$$
$$= \dot{m}_{r,e,int1} - \dot{m}_{r,e,out} \tag{6.22}$$

Evaporator Conservation of Refrigerant Energy (Two-Phase and Superheat Regions)

$$\left[\frac{d(\rho_{r,l}h_{r,l})}{dP_e}(1-\bar{\gamma})+\frac{d(\rho_{r,v}h_{r,v})}{dP_e}\bar{\gamma}-1\right]A_{e,cs}L_{e,1}\dot{P}_e+(\rho_{r,l}h_{r,l}-\rho_{r,v}h_{r,v})(1-\bar{\gamma})A_{e,cs}\dot{L}_{e,1}$$
$$=\dot{m}_{r,e,in}h_{r,e,in}-\dot{m}_{r,e,int1}h_{r,v}+\alpha_{i,e,1}A_{i,e}\frac{L_{e,1}}{L_{e,Total}}(T_{e,w1}-T_{e,r1}) \tag{6.23}$$

$$\left[\left(\left.\frac{\partial\rho_{r,e2}}{\partial P_e}\right|_{h_{r,e2}}+\frac{1}{2}\left.\frac{\partial\rho_{r,e2}}{\partial h_{r,e2}}\right|_{P_e}\frac{dh_{r,v}}{dP_e}\right)h_{r,e2}+\frac{1}{2}\frac{dh_{r,v}}{dP_e}\rho_{r,e2}-1\right]A_{e,cs}L_{e,2}\dot{P}_e+$$
$$\left[\left.\frac{\partial\rho_{r,e2}}{\partial h_{r,e2}}\right|_{P_e}h_{r,e2}+\rho_{r,e2}\right]\frac{1}{2}A_{e,cs}L_{e,2}\dot{h}_{r,e,out}+(\rho_{r,v}h_{r,v}-\rho_{r,e2}h_{r,e2})A_{e,cs}\dot{L}_{e,1} \tag{6.24}$$
$$=\dot{m}_{r,e,int1}h_{r,v}-\dot{m}_{r,e,out}h_{r,out}+\alpha_{i,e,2}A_{i,e}\frac{L_{e,2}}{L_{e,Total}}(T_{e,w2}-T_{e,r2})$$

Evaporator Conservation of Wall Energy (Two-Phase and Superheat Regions)

$$(C_p\rho V)_w\dot{T}_{e,w1}=\alpha_{o,e}A_{o,e}(T_{a,e,avg}-T_{e,w1})-\alpha_{i,e,1}A_{i,e}(T_{e,w1}-T_{e,r1}) \tag{6.25}$$

$$(C_p\rho V)_w\left[\dot{T}_{e,w2}-\left(\frac{T_{e,w2}-T_{e,w1}}{L_{e,2}}\right)\dot{L}_{e,1}\right]=\alpha_{o,e}A_{o,e}(T_{a,e,avg}-T_{e,w2})-\alpha_{i,e,2}A_{i,e}(T_{e,w2}-T_{e,r2}) \tag{6.26}$$

Condenser Conservation of Refrigerant Mass (Superheat, Two-Phase and Subcool Regions)

$$(\rho_{r,c1}-\rho_{r,v})A_{c,cs}\dot{L}_{c,1}+\left[\left.\frac{\partial\rho_{r,c1}}{\partial P_c}\right|_{h_{r,c1}}+\frac{1}{2}\left.\frac{\partial\rho_{r,c1}}{\partial h_{r,c1}}\right|_{P_c}\frac{dh_{r,v}}{dP_c}\right]A_{c,cs}L_{c,1}\dot{P}_c+$$
$$\frac{1}{2}\left.\frac{\partial\rho_{r,c1}}{\partial h_{r,c1}}\right|_{P_c}A_{c,cs}L_{c,1}\dot{h}_{r,c,in}=\dot{m}_{r,c,in}-\dot{m}_{r,c,int1} \tag{6.27}$$

$$(\rho_{r,v}-\rho_{r,l})A_{c,cs}\dot{L}_{c,1}+(\rho_{r,v}-\rho_{r,l})\bar{\gamma}A_{c,cs}\dot{L}_{c,2}+\left[\frac{d\rho_{r,l}}{dP_c}(1-\bar{\gamma})+\frac{d\rho_{r,v}}{P_c}\bar{\gamma}\right]A_{c,cs}L_{c,2}\dot{P}_c = \dot{m}_{r,c,int1}-\dot{m}_{r,c,int2} \tag{6.28}$$

$$A_{c,cs}(\rho_{r,l}-\rho_{r,c3})(\dot{L}_{c,1}+\dot{L}_{c,2})+\left[\left.\frac{\partial\rho_{r,c3}}{\partial P_c}\right|_{h_{r,c3}}+\frac{1}{2}\left.\frac{\partial\rho_{r,c3}}{\partial h_{r,c3}}\right|_{P_c}\frac{dh_{r,l}}{dP_c}\right]A_{c,cs}L_{c,3}\dot{P}_c +\frac{1}{2}\left.\frac{\partial\rho_{r,c3}}{\partial h_{r,c3}}\right|_{P_c}A_{c,cs}L_{c,3}\dot{h}_{c,out}=\dot{m}_{r,c,int2}-\dot{m}_{r,c,out} \tag{6.29}$$

Condenser Conservation of Refrigerant Energy (Superheat, Two-Phase and Subcool Regions)

$$\left[\left(\left.\frac{\partial\rho_{r,c1}}{\partial P_c}\right|_{h_{r,c1}}+\frac{1}{2}\left.\frac{\partial\rho_{r,c1}}{\partial h_{r,c1}}\right|_{P_c}\frac{dh_{r,v}}{dP_c}\right)h_{r,c1}+\frac{1}{2}\frac{dh_{r,v}}{dP_c}\rho_{r,c1}-1\right]A_{c,cs}L_{c,1}\dot{P}_c +\left[\left.\frac{\partial\rho_{r,c1}}{\partial h_{r,c1}}\right|_{P_c}h_{r,c1}+\rho_{r,c1}\right]\frac{1}{2}A_{c,cs}L_{c,1}\dot{h}_{r,c,in}+(\rho_{r,c1}h_{r,c1}-\rho_{r,v}h_{r,v})A_{c,cs}\dot{L}_{c,1} = \dot{m}_{r,c,in}h_{r,c,in}-\dot{m}_{r,c,int1}h_{r,v}+\alpha_{i,c,1}A_{i,c}\frac{L_{c,1}}{L_{c,Total}}(T_{c,w1}-T_{c,r1}) \tag{6.30}$$

$$(\rho_{r,v}h_{r,v}-\rho_{r,l}h_{r,l})A_{c,cs}\dot{L}_{c,1}+(\rho_{r,v}h_{r,v}-\rho_{r,l}h_{r,l})\bar{\gamma}A_{c,cs}\dot{L}_{c,2}+\left[\frac{d(\rho_{r,l}h_{r,l})}{dP_c}(1-\bar{\gamma})+\frac{d(\rho_{r,v}h_{r,v})}{dP_c}\bar{\gamma}-1\right]A_{c,cs}L_{c,2}\dot{P}_c = \dot{m}_{r,c,int1}h_{r,v}-\dot{m}_{r,c,int2}h_{r,l}+\alpha_{i,c,2}A_{i,c}\frac{L_{c,2}}{L_{c,Total}}(T_{c,w2}-T_{c,r2}) \tag{6.31}$$

$$\left[\left(\left.\frac{\partial\rho_{r,c3}}{\partial P_c}\right|_{h_{r,c3}}+\frac{1}{2}\left.\frac{\partial\rho_{r,c3}}{\partial h_{r,c3}}\right|_{P_c}\frac{dh_{r,v}}{dP_c}\right)h_{r,c3}+\frac{1}{2}\frac{dh_{r,v}}{dP_c}\rho_{r,c3}-1\right]A_{c,cs}L_{c,3}\dot{P}_c +\left[\left.\frac{\partial\rho_{r,c3}}{\partial h_{r,c3}}\right|_{P_c}h_{r,c3}+\rho_{r,c3}\right]\frac{1}{2}A_{c,cs}L_{c,3}\dot{h}_{c,out}+A_{c,cs}(\rho_{r,l}h_{r,l}-\rho_{r,c3}h_{r,c3})(\dot{L}_{c,1}+\dot{L}_{c,2}) = \dot{m}_{r,c,int2}h_{r,l}-\dot{m}_{r,c,out}h_{c,out}+\alpha_{i,c,3}A_{i,c}\frac{L_{c,3}}{L_{c,Total}}(T_{c,w3}-T_{c,r3}) \tag{6.32}$$

Condenser Conservation of Wall Energy (Superheat, Two-Phase and Subcool Regions)

$$(mC_p)_w\dot{T}_{c,w1} + (mC_p)_w\frac{T_{c,w1} - T_{c,w2}}{L_{c,1}}\dot{L}_{c,1} = \alpha_{o,c}A_{o,c}(T_{a,c,avg} - T_{c,w1}) - \alpha_{i,c,1}A_{i,c}(T_{c,w1} - T_{c,r1}) \tag{6.33}$$

$$(mC_p)_w\dot{T}_{c,w2} = \alpha_{o,c}A_{o,c}(T_{a,c,avg} - T_{c,w2}) - \alpha_{i,c,2}A_{i,c}(T_{c,w2} - T_{c,r2}) \tag{6.34}$$

$$(mC_p)_w\dot{T}_{c,w3} + (mC_p)_w\frac{T_{c,w1} - T_{c,w2}}{L_{c,1}}(\dot{L}_{c,1} + \dot{L}_{c,2}) = \alpha_{o,c}A_{o,c}(T_{a,c,avg} - T_{c,w3}) - \alpha_{i,c,3}A_{i,c}(T_{c,w3} - T_{c,r3} \tag{6.35}$$

Once all the ODEs were formed for each heat exchanger, there are more equations that state variables (For the evaporator, 6 equations, 5 state variables; For the condenser, 9 equations, 7 state variables). This allows the conservation equations to be combined for each heat exchanger, to eliminate $\dot{m}_{r,e,int1}$ in the case of the evaporator conservation equations and $\dot{m}_{r,c,int1}$ and $\dot{m}_{r,c,int2}$ for the condenser conservation equations. The terms of these new equations correspond to the elements of the Z(x,u) and f(x,u) matrices for the evaporator and condenser. These matrices are presented in Equations 6.36-6.37 with the matrix elements described in Tables 6.1 - 6.4. [Rasmussen [2005]].

$$\begin{bmatrix} z_{e_{1,1}} & z_{e_{1,2}} & 0 & 0 & 0 \\ z_{e_{2,1}} & z_{e_{2,2}} & z_{e_{2,3}} & 0 & 0 \\ z_{e_{3,1}} & z_{e_{3,2}} & z_{e_{3,3}} & 0 & 0 \\ 0 & 0 & 0 & z_{e_{4,4}} & 0 \\ z_{e_{5,1}} & 0 & 0 & 0 & z_{e_{5,5}} \end{bmatrix} \begin{bmatrix} \dot{L}_{e,1} \\ \dot{P}_e \\ \dot{h}_{r,e,out} \\ \dot{T}_{e,w1} \\ \dot{T}_{e,w2} \end{bmatrix} = \begin{bmatrix} f_{e_1} \\ f_{e_2} \\ f_{e_3} \\ f_{e_4} \\ f_{e_5} \end{bmatrix} \tag{6.36}$$

$z_{e_{1,1}}$	$\rho_{r,l}\ (h_{r,l}$ - $h_{r,v})\ (1\text{-}\bar{\gamma})\ A_{e,cs}$
$z_{e_{1,2}}$	$\left[\left(\frac{d(\rho_{r,l}h_{r,l})}{dP_e} - \frac{d\rho_{r,l}}{dP_e}h_{r,v}\right)(1-\bar{\gamma}) + \left(\frac{d(\rho_{r,v}h_{r,v})}{dP_e} - \frac{d\rho_{r,v}}{dP_e}h_{r,v}\right)(\bar{\gamma}) - 1\right]\ A_{e,cs}\ L_{e,1}$
$z_{e_{2,1}}$	$\rho_{r,e2}\ (h_{r,v}$ -$h_{r,e2})\ A_{e,cs}$
$z_{e_{2,2}}$	$\left[\left(\frac{\partial\rho_{r,e2}}{\partial P_e}\Big\vert_{h_{r,e2}} + \frac{1}{2}\frac{\partial\rho_{r,e2}}{\partial h_{r,e2}}\Big\vert_{P_e}\frac{dh_{r,v}}{dP_e}\right)(h_{r,e2}-h_{r,v}) + \frac{\rho_{r,e2}}{2}\frac{dh_{r,v}}{dP_e} - 1\right]\ A_{e,cs}\ L_{e,2}$
$z_{e_{2,3}}$	$\left[\frac{1}{2}\frac{\partial\rho_{r,e2}}{\partial h_{r,e2}}\Big\vert_{P_e}(h_{r,e2}-h_{r,v}) + \frac{\rho_{r,e2}}{2}\right]\ A_{e,cs}\ L_{e,2}$
$z_{e_{3,1}}$	$[(\rho_{r,v}$ - $\rho_{r,e2})$ + $(\rho_{r,l}$ - $\rho_{r,v})\ (1\text{-}\bar{\gamma})]\ A_{e,cs}$
$z_{e_{3,2}}$	$\left[\left(\frac{\partial\rho_{r,e2}}{\partial P_e}\Big\vert_{h_{r,e2}} + \frac{1}{2}\frac{\partial\rho_{r,e2}}{\partial h_{r,e2}}\Big\vert_{P_e}\frac{dh_{r,v}}{dP_e}\right)L_{e,2} + \left(\frac{d\rho_{r,l}}{dP_e}(1-\bar{\gamma}) + \frac{d\rho_{r,v}}{dP_e}\bar{\gamma}\right)L_{e,1}\right]\ A_{e,cs}$
$z_{e_{3,3}}$	$\frac{1}{2}\ \frac{\partial\rho_{r,2}}{\partial h_{r,e2}}\Big\vert_{P_e}\ A_{e,cs}\ L_{e,2}$
$z_{e_{4,4}}$	$(C_p\rho V)_w$
$z_{e_{5,1}}$	$(C_p\rho V)_w\ \left(\frac{T_{e,w1}-T_{e,w2}}{L_{e,2}}\right)$
$z_{e_{5,5}}$	$(C_p\rho V)_w$

Table 6.1: Evaporator Z(x,u) Elements

f_{e_1}	$\dot{m}_{r,e,in}\ (h_{r,e,in}$ - $h_{r,v})$ + $\alpha_{i,e,1}\ A_{i,e}\ \frac{L_{e,1}}{L_{e,Total}}(\ T_{e,w1}$ - $T_{e,r1})$
f_{e_2}	$\dot{m}_{r,e,out}\ (h_{r,v}$ - $h_{r,e,out})$ + $\alpha_{i,e,2}\ A_{i,e}\ \frac{L_{e,2}}{L_{e,Total}}\ (T_{e,w2}$ - $T_{e,r2})$
f_{e_3}	$\dot{m}_{r,e,in}$ - $\dot{m}_{r,e,out}$
f_{e_4}	$\alpha_{o,e}\ A_{o,e}(T_{a,e,avg}$ - $T_{e,w1})$ - $\alpha_{i,e,1}\ A_{i,e}\ (T_{e,w1}$ - $T_{e,r1})$
f_{e_5}	$\alpha_{o,e}\ A_{o,e}\ (T_{a,e,avg}$ - $T_{e,w2})$ - $\alpha_{i,e,2}\ A_{i,e}\ (T_{e,w2}$ - $T_{e,r2})$

Table 6.2: Evaporator f(x,u) Elements

$$\begin{bmatrix} z_{c_{1,1}} & 0 & z_{c_{1,3}} & 0 & 0 & 0 & 0 \\ z_{c_{2,1}} & z_{c_{2,2}} & z_{c_{2,3}} & z_{c_{2,4}} & 0 & 0 & 0 \\ z_{c_{3,1}} & z_{c_{3,2}} & z_{c_{3,3}} & z_{c_{3,4}} & 0 & 0 & 0 \\ z_{c_{4,1}} & z_{c_{4,2}} & z_{c_{4,3}} & z_{c_{4,4}} & 0 & 0 & 0 \\ z_{c_{5,1}} & 0 & 0 & 0 & z_{c_{5,5}} & 0 & 0 \\ 0 & 0 & 0 & 0 & 0 & z_{c_{6,6}} & 0 \\ z_{c_{7,1}} & z_{c_{7,2}} & 0 & 0 & 0 & 0 & z_{c_{7,7}} \end{bmatrix} \begin{bmatrix} \dot{L}_{c,1} \\ \dot{L}_{c,2} \\ \dot{P}_c \\ \dot{h}_{c,out} \\ \dot{T}_{c,w1} \\ \dot{T}_{c,w2} \\ \dot{T}_{c,w3} \end{bmatrix} = \begin{bmatrix} f_{c_1} \\ f_{c_2} \\ f_{c_3} \\ f_{c_4} \\ f_{c_5} \\ f_{c_6} \\ f_{c_7} \end{bmatrix} \tag{6.37}$$

$z_{c_{1,1}}$	$\rho_{r,c1}\ (h_{r,c1}$ - $h_{r,v})\ A_{c,cs}$
$z_{c_{1,3}}$	$\left[\left(\frac{\partial\rho_{r,c1}}{\partial P_c}\Big\vert_{h_{r,c1}} + \frac{1}{2}\frac{\partial\rho_{r,c1}}{\partial h_{r,c1}}\Big\vert_{P_c}\frac{dh_{r,v}}{dP_c}\right)(h_{r,c1}-h_{r,v}) + \frac{1}{2}\frac{dh_{r,v}}{dP_c}\rho_{r,c1} - 1\right] A_{c,cs}\ L_{c,1}$
$z_{c_{2,1}}$	$(\rho_{r,c1}\ h_{r,v}$ - $\rho_{r,c3}\ h_{r,l})\ A_{c,cs}$
$z_{c_{2,2}}$	$[\ (\rho_{r,v}\ h_{r,v}$ - $\rho_{r,l}\ h_{r,l})\ \bar{\gamma} + (\rho_{r,l}$ - $\rho_{r,c3})\ h_{r,l}]\ A_{c,cs}$
$z_{c_{2,3}}$	$\left(\frac{\partial\rho_{r,c1}}{\partial P_c}\Big\vert_{h_{r,c1}} + \frac{1}{2}\frac{\partial\rho_{r,c1}}{\partial h_{r,c1}}\Big\vert_{P_c}\frac{dh_{r,v}}{dP_c}\right) h_{r,v}\ L_{c,1}\ A_{c,cs} + \left(\frac{d(\rho_{r,l}h_{r,l})}{dP_c}(1-\bar{\gamma}) + \frac{d(\rho_{r,v}h_{r,v})}{dP_c}\bar{\gamma} - 1\right) L_{c,2}\ A_{c,c}$ $+ \left(\frac{\partial\rho_{r,c3}}{\partial P_c}\Big\vert_{h_{r,c3}} + \frac{1}{2}\frac{\partial\rho_{r,c3}}{\partial h_{r,c3}}\Big\vert_{P_c}\frac{dh_{r,l}}{dP_c}\right) h_{r,l}\ L_{c,3}\ A_{c,cs}$
$z_{c_{2,4}}$	$\frac{1}{2}\ \frac{\partial\rho_{r,c3}}{\partial h_{r,c3}}\Big\vert_{P_c}\ L_{c,3}\ A_{c,cs}\ h_{r,l}$
$z_{c_{3,1}}$	$\rho_{r,c3}\ (h_{r,l}$ - $h_{r,c3})\ A_{c,cs}$
$z_{c_{3,2}}$	$\rho_{r,c3}\ (h_{r,l}$ - $h_{r,c3})\ A_{c,cs}$
$z_{c_{3,3}}$	$\left[\left(\frac{\partial\rho_{r,c3}}{\partial P_c}\Big\vert_{h_{r,c3}} + \frac{1}{2}\frac{\partial\rho_{r,c3}}{\partial h_{r,c3}}\Big\vert_{P_c}\frac{dh_{r,l}}{dP_c}\right)(h_{r,c3}-h_{r,l}) + \frac{1}{2}\frac{dh_{r,l}}{dP_c}\rho_{r,c3} - 1\right] A_{c,cs}\ L_{c,3}$
$z_{c_{3,4}}$	$\left[\frac{1}{2}\frac{\partial\rho_{r,c3}}{\partial h_{r,c3}}\Big\vert_{P_c}(h_{r,c3}-h_{r,l}) + \frac{1}{2}\rho_{r,c3}\right] L_{c,3}\ A_{c,cs}$
$z_{c_{4,1}}$	$(\rho_{r,c1}$ - $\rho_{r,c3})\ A_{c,cs}$
$z_{c_{4,2}}$	$[\ (\rho_{r,v}$ - $\rho_{r,l})\ \bar{\gamma} + (\rho_{r,l}$ - $\rho_{r,c3})\ ]\ A_{c,cs}$
$z_{c_{4,3}}$	$\left(\frac{\partial\rho_{r,c1}}{\partial P_c}\Big\vert_{h_{r,c1}} + \frac{1}{2}\frac{\partial\rho_{r,c1}}{\partial h_{r,c1}}\Big\vert_{P_c}\frac{dh_{r,v}}{dP_c}\right) L_{c,1}\ A_{c,cs} + \left(\frac{d\rho_{r,l}}{dP_c}(1-\bar{\gamma}) + \frac{d\rho_{r,v}}{P_c}\bar{\gamma}\right) L_{c,2}\ A_{c,cs}$ $+ \left(\frac{\partial\rho_{r,c3}}{\partial P_c}\Big\vert_{h_{r,c3}} + \frac{1}{2}\frac{\partial\rho_{r,c3}}{\partial h_{r,c3}}\Big\vert_{P_c}\frac{dh_{r,l}}{dP_c}\right) L_{c,3}\ A_{c,cs}$
$z_{c_{4,4}}$	$\frac{1}{2}\ \frac{\partial\rho_{r,c3}}{\partial h_{r,c3}}\ A_{c,cs}\ L_{c,3}$
$z_{c_{5,1}}$	$(mC_p)_w\ \frac{T_{c,w1}-T_{c,w2}}{L_{c,1}}$
$z_{c_{5,5}}$	$(mC_p)_w$
$z_{c_{6,6}}$	$(mC_p)_w$
$z_{c_{7,1}}$	$(mC_p)_w\ \frac{T_{c,w2}-T_{c,w3}}{L_{c,3}}$
$z_{c_{7,2}}$	$(mC_p)_w\ \frac{T_{c,w2}-T_{c,w3}}{L_{c,3}}$
$z_{c_{7,7}}$	$(mC_p)_w$

Table 6.3: Condenser Z(x,u) Elements

f_{c_1}	$\dot{m}_{r,c,in}\ (h_{r,c,in}$ - $h_{r,v}) + \alpha_{i,c,1}\ A_{i,c}\ \frac{L_{c,1}}{L_{c,Total}}(\ T_{c,w1}$ - $T_{c,r1})$
f_{c_2}	$\dot{m}_{r,c,in}\ h_{r,v}$ - $\dot{m}_{r,c,out}\ h_{r,l} + \alpha_{i,c,2}\ A_{i,c}\ \frac{L_{c,2}}{L_{c,Total}}(\ T_{c,w2}$ - $T_{c,r2})$
f_{c_3}	$\dot{m}_{r,c,out}\ (h_{r,l}$ - $h_{c,out}) + \alpha_{i,c,3}\ A_{i,c}\ \frac{L_{c,3}}{L_{c,Total}}(\ T_{c,w3}$ - $T_{c,r3})$
f_{c_4}	$\dot{m}_{r,c,in}$ - $\dot{m}_{r,c,out}$
f_{c_5}	$\alpha_{o,c}\ A_{o,c}(T_{a,c,avg}$ - $T_{c,w1})$ - $\alpha_{i,c,1}\ A_{i,c}\ (T_{c,w1}$ - $T_{c,r1})$
f_{c_6}	$\alpha_{o,c}\ A_{o,c}(T_{a,c,avg}$ - $T_{c,w2})$ - $\alpha_{i,c,2}\ A_{i,c}\ (T_{c,w2}$ - $T_{c,r2})$
f_{c_7}	$\alpha_{o,c}\ A_{o,c}(T_{a,c,avg}$ - $T_{c,w3})$ - $\alpha_{i,c,3}\ A_{i,c}\ (T_{c,w3}$ - $T_{c,r3})$

Table 6.4: Condenser f(x,u) Elements

Note: All these equations were obtained from Rasmussen [2005].

B Openloop Step Responses at different Operating Points

In Figure 6.1(a) and 6.1(b), T_{SA} responses corresponding to a lower final steady state value correspond to a higher nominal valve opening value and a higher nominal RPM value, respectively.

In Figure 6.2(a) and 6.2(b), T_{SH} responses corresponding to a lower final steady state value correspond to a higher nominal valve opening value and a lower nominal RPM value, respectively.

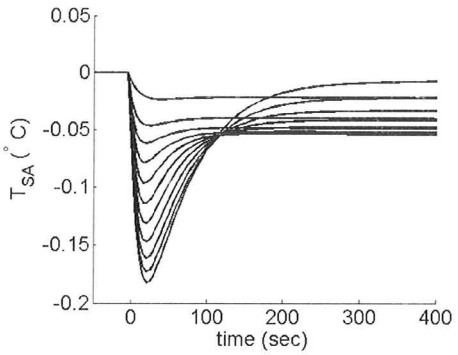

(a) T_{SA}-RPM

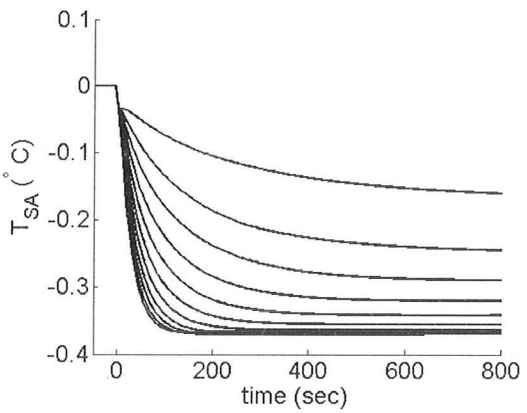

(b) T_{SA}-Valve

Figure 6.1: T_{SH} Responses to RPM and Valve step changes

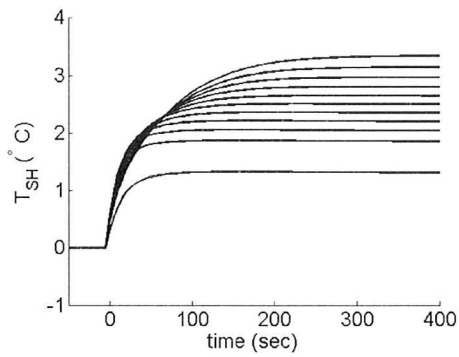

(a) T_{SH}-RPM

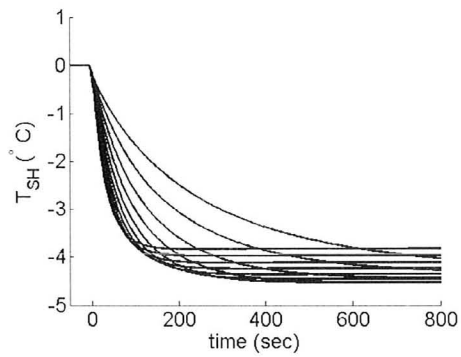

(b) T_{SH}-Valve

Figure 6.2: T_{SH} Responses to RPM and Valve step changes